November 1986
LU TP 86-24

A Comparative Study of Coherent and Non-Coherent Parton Shower Evolution

Mats Bengtsson, Torbjörn Sjöstrand
Department of Theoretical Physics,
University of Lund, Sölvegatan 14 A,
S-223 62 Lund, Sweden

Abstract:
We present a new algorithm for the probabilistic evolution of jet cascades, based on the leading log approximation to perturbative QCD, augmented by coherence studies. Compared to previous models, emphasis is put on expressing kinematical variables in terms of Lorentz invariants and on matching on to the three-jet matrix element in e^+e^- annihilation. A systematic study is made of various assumptions in the model, such as the implementation of kinematics, the choice of Q^2 scale and the inclusion of angular ordering. In particular, we address the issue of how to find experimental evidence for coherence effects.

1 Introduction

Standard QCD perturbation theory is based on the calculation of matrix elements, expanded in orders of α_s. In e^+e^- annihilation, the best understood process, this program has been carried out to second order in α_s [1]. Calculations to higher orders are increasingly difficult, so that the hope for such results seems small. For energies higher than present ones, the data should reflect the increased probability for multigluon bremsstrahlung, in a way that probably can not be reproduced only by the usage of 2-, 3- and 4-parton states. In a parton shower approach, on the other hand, basic $q \to qg$, $g \to gg$ and $g \to q\bar{q}$ branchings may be iterated to describe the production of an arbitrary number of partons in the final state. The price to be paid is the introduction of a number of approximations; in particular wide angle emission may be less accurately described.

While the breakdown of a matrix element approach at higher energies is uncontroversial, at present energies the phenomenological need for parton showers rather than matrix elements is not obvious. In [2] we argue that experimental data indeed points to shortcomings in the matrix element approach. This conclusion is based on the difference in quark and gluon jet fragmentation functions, on the four-jet rate, and on the energy-energy correlation asymmetry at small angles, all of which are better described with parton showers.

By now, a number of models for timelike (final state) parton showers have been developed. Early models [3-6], here called "conventional" or "non-coherent" ones, were incomplete in the sense that they did not correctly take into account soft gluon interference effects [7]. The first example of a "coherent" model, that does include these effects, was the Marchesini-Webber (MW) one [8]. The practical implementation here is awkward, however, in that the invariant mass of the parton system is not known beforehand. Furthermore, the model is not explicitly Lorentz covariant, and the choice of evolution variable is not transparent.

Instead we develop a somewhat different algorithm, that avoids these particular problems. Some other problems do appear, but less serious ones, we feel. Anyhow, comparisons between different implementations will provide consistency checks and a better understanding of details. In particular, our

algorithm allows us to study the importance of different definitions of the z splitting variable, different choices of α_s argument, and the inclusion or not of angular ordering, one component at a time. This way we hope to shed some light on which features truly distinguish conventional and coherent branching models in a broader sense, rather than just one particular conventional algorithm from another particular coherent one.

It is often claimed that the "string effect", first observed by JADE [9] and later by several other collaborations [10,11], is evidence for the necessity to include coherence in the branching process. We will study this issue in some detail, and show that the situation is actually a bit more complicated; if a string fragmentation scheme [12] is used, also a non-coherent parton shower may exhibit the string effect. This in no way casts doubt on the coherence phenomenon as such, it is just an indication that explicit proof are hard to come by at present energies. A method is developed for the study of angular ordering, one of the cornerstones of coherence phenomenology, but in reality it can only be applied for CM energies above 100 GeV. On the other hand, it is amusing to note that current data not only favours a running α_s, that depends on the individual branching kinematics also for fixed CM energy, but furthermore that the Q^2 scale in $\alpha_s(Q^2)$ should be p_T^2 rather than m^2, i.e. in agreement with coherence predictions.

Detailed studies of the kind outlined above can not be carried out by analytical techniques. Rather we have used the Monte Carlo approach to write a computer program for the explicit simulation of shower evolution. This way complete events are generated, that can be analyzed in detail. The program is publicly available within the framework of the Lund Monte Carlo for Jet Fragmentation and e^+e^- Physics, JETSET version 6.3 [13,14].

The outline of this paper is as follows. In section 2 the principles for parton showers are reviewed and the special features of our model are described in detail. Some of the standard phenomenology at present e^+e^- energies is investigated in section 3, with special emphasis on the string effect. Section 4 deals mainly with questions of a more theoretical nature, such as multiplicity growth with energy. We extrapolate to higher energies and search for coherence effects that can manifest themselves in experimentally measurable particle distributions. Section 5 deals with differences between gluon and quark jets, with an imagined toponium at 50 GeV contrasted to the continuum background. A conclusion ends the paper.

2 The Model

A number of papers and review articles on theoretical issues and earlier models exist [3-6,15]. We will in section 2.1 repeat the basic formulae and comment upon open issues. The details of our model are presented in section 2.2, and in section 2.3 we discuss the question of fragmentation and the adjustments of details in the fragmentation process.

2.1 The Formalism

The formalism used for generating parton showers, once the meaning of the variables has been defined, is by now standard but will be reviewed briefly in the following. A parton shower can be looked upon as a tree with quark and gluon lines as branches. Three different branchings are possible, $q \to qg$, $g \to gg$ and $g \to q\bar{q}$, associated with the Altarelli-Parisi (AP) evolution equations [16]

$$dP_{a\to bc} = \frac{\alpha_s(Q^2)}{2\pi} \frac{dm_a^2}{m_a^2} P_{a\to bc}(z)\, dz \tag{1}$$

where the $P_{a\to bc}(z)$ is the splitting kernel, characteristic for the type of branching

$$P_{q\to qg}(z) = \frac{4}{3}\frac{1+z^2}{1-z}$$

$$P_{g\to gg}(z) = \frac{6(1-z(1-z))^2}{z(1-z)}$$

$$P_{g\to q\bar{q}}(z) = \frac{1}{2}\,(z^2+(1-z)^2) \quad . \tag{2}$$

The argument in α_s, Q^2, is generally a function of both m_a^2 and z. The probability that a parton does not branch between some initial maximum mass m^2 and a minimum mass m_{min}^2 is given by the exponentiation of (1)

$$S_a(m^2) = \exp\left\{ -\int_{m_{min}^2}^{m^2} \frac{dm'^2}{m'^2} \int_{z_-(m')}^{z_+(m')} \frac{\alpha_s(Q^2)}{2\pi}\, dz\, P_{a\to bc}(z) \right\} \tag{3}$$

called the Sudakov form factor. To regularize collinear divergences (in z) and infrared divergences (in m^2) one has to introduce a small cutoff scale, m_{min}, which will be discussed further. The z_- and z_+ values depend on m_{min} in a functional form related to the precise definition of z. The probability

distribution $p_a(m_{max}^2, m^2)$ that a parton with a maximum allowed virtuality m_{max}^2 will actually obtain a virtuality between m^2 and m^2+dm^2 is then

$$p_a(m_{max}^2, m^2)\, dm^2 = S_a(m_{max}^2) \frac{d}{dm^2}\left\{\frac{1}{S_a(m^2)}\right\} dm^2 \quad . \tag{4}$$

Branches are generated by solving for m :

$$S_a(m^2) = \frac{S_a(m_{max}^2)}{R} \tag{5}$$

where R is a random number between 0 and 1. The solution is generally not possible to obtain as an explicit expression. Instead the "veto algorithm" is used, as follows. The integrand in S_a is generally a complicated function $f(m^2)$, i.e. $S_a(m^2) = \exp(-\int f(m'^2)dm'^2)$. Assume a simpler function $g(m^2)$ may be found, with $g(m^2) \geq f(m^2)$ for all relevant m^2 values, such that the integrand $\int g(m'^2)dm'^2$ can be inverted. Then eq. (5), with $g(m^2)$ substituted for $f(m^2)$ in $S_a(m^2)$, may be inverted to yield a m^2 value. This value is accepted with probability $f(m^2)/g(m^2)$. If rejected, the procedure is repeated, but with the m^2 value just rejected as upper limit m_{max}^2. Whenever a value $m < m_{min}$ is selected, the procedure is stopped and the parton is put on mass-shell. Using $P_{a\to bc}(z)$, the splitting variable z is generated between the limits z_- and z_+. The daughters, b and c, are later allowed to branch in exactly the same way. With daughter masses m_b and m_c known, the four-momenta p_b and p_c are straightforward to construct.

The coherence effect originates from destructive interference between Feynman diagrams in a certain approximation (leading log) and is equivalent to an ordering of consecutive opening angles ($\theta_b < \theta_a$, $\theta_c < \theta_a$ if $a \to bc$) [7]. The phenomenological criticism against conventional parton showers can basically be formulated in three points: the multiplicity growth with energy is to big, the rapidity dip in the central region is absent or is too small because of a surplus of gluons at small x and the energy-energy correlation at high energy and angles close to 180° does not fit analytical predictions. One further advantage with the coherent evolution is that the available phase space (given by z_- and z_+) is not so sensitive to the precise definition of the z variable since the angular ordering condition usually sets stronger limits.

The possible choices of the evolution variable includes a function of z times m^2. An example of this is the ξ variable of MW [8], $\xi = (p_1p_2)/(E_1E_2)$. With z defined as energy fraction one gets

$$m_a^2 = m_b^2 + m_c^2 + 2E_a^2 z(1-z)\xi \tag{6}$$

and asymptotically $m_a^2 = 2E_a^2 z(1-z)\xi$. The Jacobian for the transformation from m^2 to ξ is unity, i.e. $d\ln(\xi)dz = d\ln(m^2)dz$. However there are some drawbacks with this method. Parton virtualities are not known during the evolution, but instead have to be constructed afterwards, by moving backward from daughters to mothers as seen from eq. (6). There is then no possibility to fix the invariant mass of the system beforehand. The treatment is not explicity Lorentz covariant and, as one result of this, one has to deal with an arbitrary initial opening angle. Furthermore, a complicated 3-pass process is needed for kinematics reconstruction. The advantage is that with ξ as evolution variable, coherence effects are straightforward to include: asymptotically, $\xi \approx (1-\cos\theta)$ and an ordering in ξ is equivalent to an ordering in θ. Angular ordering can be obtained without using this awkward variable, however, and we will follow a different approach.

To construct a model for parton showers, there are basically three important decisions to be made: the choice of evolution variable, the definition of splitting variable z and the related treatment of kinematics, and the use of Q^2 scale in α_s. The usual choice of evolution variable is m^2 but, as we have seen, a function of z times m^2 will do. The leading log approximation is strictly valid only in the domain where the masses are strongly ordered, $m_j^2 >> m_{j-1}^2$. Here all definitions of z should agree. However, differences arise in the domain where $m_{j-1}^2 \sim O(m_j^2)$, which occurs frequently in reality. Therefore a careful choice of z can mimic nonleading contributions to the branching process. Finally, a study of coherence effects has shown that the proper choice for Q^2 scale in α_s is $p_T^2 \approx z(1-z)m^2$ rather than m^2 [17]. Also this turns out to be of some importance.

2.2 Our Model

The choice of z definition is constrained by the desire to keep the treatment explicitly Lorentz covariant, and also to agree as closely as possible with the structure of the lowest order three-jet matrix element. Consider an e^+e^- annihilation event, with the branches of the shower numbered as in Fig. 1. The definition of z_1 in the branching $q_1 \to q_3 + g_4$ is then

$$z_1 = \frac{p_0 p_3}{p_0 p_1} = \frac{E_3}{E_1} \tag{7}$$

the latter equality valid in the rest frame of the virtual photon, i.e. for $p_0 = (W,\bar{0})$. This z expression is formally Lorentz invariant, but p_0 acts as a "gauge fixing" vector. As a natural consequence of momentum conservation one has "z_1" + "$1-z_1$" = $E_3/E_1 + E_4/E_1 = 1$.

For comparisons with the three-jet matrix element, insert $z = E_3/E_1 = x_q/(x_q + x_g)$ and $m^2 = (1-x_{\bar{q}})W^2$ in the combined probability function

$$dP_{q^*\to qg}(m^2,z) = \frac{\alpha_s(Q^2)}{2\pi}\frac{dm^2}{m^2}\frac{4}{3}\frac{1+z^2}{1-z}\,dz\ . \tag{8}$$

and sum with the corresponding expression for $\bar{q}^* \to \bar{q}g$ ($x_i = 2E_i/W$). As was shown in [2], the result has exactly the same singularity structure as the matrix element, coincides with it when $x_1 \to 1$ or $x_2 \to 1$, and elsewhere overestimates it by most a factor of 20/9 in the sparsely occupied region $x_1 = x_2 = 1/2$. This makes it possible to reproduce the matrix element by generating branches of parton 1 and 2 according to the shower algorithm, but accept these branches with a probability $d\sigma_{matrix}/d\sigma_{shower}$. One should note that some implicit differences remain, to the advantage of parton showers. The matrix element Q^2 scale is $Q^2 = s$, the parton shower one $Q^2 = z(1-z)m^2$ [17]. Further, in parton showers the probability of a first branching at a given m is reduced by the probability that no branching has taken place at a larger virtuality, i.e. by the Sudakov form factor.

To continue the discussion on the choice of z, two alternatives are included. For the first branch, z_1 was defined as $(p_0p_3)/(p_0p_1)$. This is equal to energy fraction in the rest frame of the grandmother, which here is the same as the total CM frame. For the following branches $3 \to 5 + 6$ etc. one may either use the grandmother's rest frame, i.e. $z_3 = (p_1p_5)/(p_1p_3)$, or stay in the total CM frame where $z_3 = (p_0p_5)/(p_0p_3)$. The former definition is in some respects more natural, but has the disadvantage that the "gauge vector" is changed during the evolution.

We have further considered two different approaches to the treatment of the kinematics, which also affects the interpretation of z. In the first case the actual masses of the daughter partons and the z value are checked for kinematical consistency, and unallowed branchings are rejected by veto techniques. As an alternative, the daughters 3 and 4 are assumed massless in

the evolution of the mother, parton 1. This approach increases the available phase space and results in a larger multiplicity growth with energy. When the masses m_3 and m_4 have been found, the four-momenta p_3 and p_4 can be constructed in a Lorentz invariant way from the massless ones p_3^0 and p_4^0 as

$$p_{3,4} = p_{3,4}^0 \pm (r_4 p_4^0 - r_3 p_3^0) \tag{9}$$

where r_3 and r_4 are chosen so that the directions of the three-momenta are unchanged in the rest frame of parton 1. Strictly speaking, in a purely probabilistic and classical approach as ours, it is an approximation to treat the daughters as massless. But in a quantized field theory as QCD, one has to be very careful in the use of classical arguments. Furthermore, the AP equations are derived in the leading log approximation and do not involve massive daughters.

In order to simplify the analysis, we have chosen not to use all the possible options (2*2) here, but instead only allow the two most extreme alternatives. When the photon four-momentum acts as a "gauge vector", i.e. the global z definition, the daughters are additionally assumed massless in the evolution of the mother. In contrast, the "local" z definition is with the respective grandmother's four-momentum acting as "gauge vector", and with the actual masses of the daughters taken into account in the evolution. The details in the evolution are different in the two cases and we therefore describe the local z case first, followed by the technically simpler global z case.

In the local z case and in the rest frame of p_0, the allowed z range $z_{1-} < z_1 < z_{1+}$ is obtained as

$$z_{1\pm} = \frac{1}{2}\left\{1 + \frac{m_3^2 - m_4^2}{m_1^2} \pm \frac{|\bar{p}_1|}{E_1}\frac{\lambda_{134}^{1/2}}{m_1^2}\right\} \tag{10}$$

with

$$\lambda_{134} = (m_1^2 - m_3^2 - m_4^2)^2 - 4m_3^2 m_4^2 \quad . \tag{11}$$

When parton 1 is evolved, its mass m_1 and splitting variable z_1 together with its branching mode (for a quark always $q \to qg$, for a gluon either $g \to gg$ or $g \to q\bar{q}$) are chosen at the same time.

For a moment assume $m_3 = m_4 = m_{eff}$ (m_{eff} is an effective cutoff mass to be defined later) which is valid asymptotically and which maximizes the z_1 interval and justifies the use of the veto algorithm. Then the limits are

$$z_{1\pm} = \frac{1}{2}\left\{1 \pm \frac{|\bar{p}_1|}{E_1}\left[1 - \frac{4m_{eff}^2}{m_1^2}\right]^{1/2}\right\} \quad . \tag{12}$$

To use the veto algorithm, an overestimation of the function in the exponent of the Sudakov form factor must be made with a simple and invertible function. Maximization with respect to m_1 gives, for $m_1^2 = 2m_{eff}E_1$,

$$\frac{m_{eff}}{E_1} < z_1 < 1 - \frac{m_{eff}}{E_1} \quad . \tag{13}$$

However, the joint distribution in m_1^2 and m_2^2 does not factorize since E_1 depends on both m_1 and m_2, $E_1 = (m_0^2 + m_1^2 - m_2^2)/2m_0$. The evolution of parton 1 and 2 therefore has to be carried out in parallel. In principle it is possible to calculate the combined probability distribution as

$$p(m_1^2, m_2^2) = \frac{f(m_1^2|m_2^2)}{\int \{f(m^2|m_2^2)/f(m_2^2|m^2)\}\, dm^2} \tag{14}$$

where $f(m_1^2|m_2^2)dm_1^2$ is the conditional probability to find an m^2 between m_1^2 and $m_1^2 + dm_1^2$ given a certain m_2^2. The $f(m_1^2|m_2^2)$ is just eq. (4) with a fixed m_2^2. In practice this is not possible and, since corrections only enter subasymptotically, we choose a simplified scheme. Start evolving both daughters p_1 and p_2 using $E_1 = E_2 = m_0$ in eq. (13), when determining m_1 and m_2, respectively. With both m_1 and m_2 chosen, the energies E_1 and E_2 are found, and z_1 and z_2 may be checked against the condition (12). If only one of z_1 or z_2 is unphysical, then that leg is evolved further. If both are unphysical, the one wich is violated most seriously (measured in terms of the integral of the AP kernel) is evolved and the checks repeated afterwards. If the chosen masses are unphysical because $m_1 + m_2 > m_0$, the question of which leg to evolve is not so simple: the veto algorithm is applicable only in the one-dimensional case. As a simple recipe, we choose to continue to evolve the one with biggest ratio $m_{present}/m_{max}$ (here $m_{max} = m_0$), because of pure symmetry reasons.

Now the daughters 3 and 4 may be evolved, subject to the constraints $m_{3max} = \min(m_1, z_1E_1)$ and $m_{4max} = \min(m_1, (1-z_1)E_1)$, but otherwise with the same recipe as for 1 and 2 above. However, with these m_3 and m_4 the allowed interval in z_1 is generally decreased, see eq. (10) and it is possible that z_1 falls outside the new limits. If it does, whichever of m_3 and m_4 has largest ratio $m_{present}/m_{max}$ is evolved further. The motivation for this procedure is as follows. When m_3 is generated, a too large range in z_3 is used, eq. (12),

instead of the correct one, eq. (10). This gives too large an integrand in the Sudakov form factor, and hence a slightly too large average mass m_3. But the generated m_3 and m_4 generally decrease the allowed range of the preceding splitting variable (z_1) in the manner just described. This in turns tend to push the masses m_3 and m_4 down, i.e. the two effects partly cancel.

Turning now to the global z case, a number of simplifications in the algorithm can be made. When the daughters 3 and 4 are assumed massless the allowed range in z_1 is

$$z_{1\pm} = \frac{1}{2}\left\{1 \pm \frac{|\bar{p}_1|}{E_1}\,\theta(m_1-m_{min})\right\} \tag{15}$$

where $\theta(x)$ is the step function. Since E_1 depends on the mass of both parton 1 and parton 2, the evolution hase to be made in parallel, as before. For the subsequent branching $1 \to 3 + 4$ $E_3^0 = z_1E_1$ and $E_4^0 = (1-z_1)E_1$. The z_3 and z_4 intervals have only to be corrected for the E_3 and E_4 reconstructed from eq. (9). In this approach the awkward coupling between daughter masses m_3 and m_4 and $z_{1\pm}$ disappears.

One degree of freedom is still left until a branch is kinematically determined. This is simply an azimuthal angle, which we have no reason to choose in any other way than isotropically. With the four-momentum p_1 of the mother, its splitting variable z_1, the daughter masses m_3 and m_4 and the azimuthal angle known, the four-momenta p_3 and p_4 may be constructed. In the frame where z_1 is defined as energy fraction $E_3 = z_1E_1$, $E_4 = (1-z_1)E_1$ and the transverse momentum p_T of 3 and 4 with respect to the 1 direction is

$$p_T^2 = \frac{4|\bar{p}_3^2||\bar{p}_4^2| - (|\bar{p}_1^2| - |\bar{p}_3^2| - |\bar{p}_4^2|)^2}{4|\bar{p}_1^2|} \quad . \tag{16}$$

As discussed before, a cutoff can be introduced in the form of a mass m_{min}, below which partons are assumed not to radiate. We have chosen to define effective parton masses as

$$m_{eff,g} = \frac{m_{min}}{2}$$

$$m_{eff,q}^2 = \frac{m_{min}^2}{4} + m_q^2 \tag{17}$$

where $m_u = m_d = 0.325$ GeV, $m_s = 0.5$ GeV, $m_c = 1.6$ GeV and $m_b = 5.0$ GeV are the ordinary quark masses. The minimum masses are then defined as

$$m_{min,g} = 2m_{eff,g} = m_{min}$$

$$m_{min,q} = m_{eff,q} + m_{eff,g} \quad . \tag{18}$$

There is a freedom to use different scales as argument in α_s. The conventional choice is here m^2, the mass-square of the decaying parton. Studies of coherence effects [17] suggest that the p_T^2 of the daughters should be more relevant. The expression for p_T^2 reduces in the asymptotic limit, where $m_3 \ll m_1$ and $m_1 \ll E_1$, to $p_T^2 \approx z_1(1-z_1)m_1^2$. In the coherent case $Q_{coh}^2 = z(1-z)m^2$ will therefore be used. For the conventional choice, $Q_{conv}^2 = m^2/4$ is used rather than just m^2, since the former coincides with Q_{coh}^2 for $z = 1/2$. The smallest value the argument can take in the conventional case is m_{eff}^2. For consistency, the perturbative evolution must be terminated at the same α_s-value in both cases. Therefore a further constraint $z(1-z)m^2 > m_{eff}^2$ is required in the coherent case. Note that the Λ value determined in the parton shower approach can not be directly equated with the $\Lambda_{\overline{MS}}$ of matrix element calculations: firstly the perturbative expansions are made in terms of different Q^2 scales, secondly the nonleading logs are not guaranteed to agree for the two.

The main effect of coherence is to introduce an "angular ordering" of successive branchings. Obviously the concept of angles is Lorentz frame dependent, so in our formalism it is convenient to rephrase angular ordering as follows. Assuming the opening angle θ_1 (for $1 \to 3 + 4$) small, one obtains

$$\theta_1 \approx \frac{m_1}{E_1[z_1(1-z_1)]^{1/2}} \tag{19}$$

valid in the frame where z_1 is defined as energy fraction. A similar expression holds for θ_3. Furthermore, one has the relation $E_3 = z_1E_1$, for the global z case with energies defined in the CM frame, for the local z one in the grandmother's (here parton 0) rest frame. In both cases the angular ordering condition $\theta_3 < \theta_1$ gives

$$\frac{z_3(1-z_3)}{m_3^2} > \frac{1-z_1}{z_1\,m_1^2} \quad . \tag{20}$$

Actually, this expression is similar to the algebraic formula that is used to prove angular ordering [7], the difference being that small z values were assumed in the original derivation, whereas the result above has been symmetrized for $z \leftrightarrow 1-z$.

The constraint in eq. (20) can be introduced into the basic parton shower formalism by an application of the veto algorithm: if eq. (20) is not fulfilled, the m_3 and z_3 values chosen are rejected and the evolution continued. Similar constraints hold for the evolution of all partons, except for the first two, where the relations $\theta_1, \theta_2 < \theta_0 = 180^0$ are fulfilled trivially (put another way, there is no z_0 in our formalism). For these branchings the matching onto the three-jet matrix element is used as a constraint instead, as described above.

2.3 Fragmentation

Turning to the question of fragmentation, there are some modifications in the parameter choices to be made due to the different partonic configurations in parton showers compared to matrix elements. A particular advantage with the string fragmentation scheme, which is used throughout, is the infrared stability: the effect on the final state of an additional gluon is vanishing whenever the gluon energy or opening angle (with respect to neighbours) goes to zero. This is necessary if one wants parameter values to vary slowly with the cutoff (m_{min}) used. The parameters in the parton shower, basically m_{min} and Λ, are treated as more fundamental than the fragmentation parameters and the latter should therefore be fitted last. Obviously, in a fully consistent picture one would not have two separate frameworks. As a consequence of this separation, there is a "grey zone" in between, a zone of medium soft gluons that can either be simulated explicitly in the parton shower or be included in the effective fragmentation parameters. Among fragmentation parameters [12,13], those related to the relative flavour production are not affected by the issues discussed here. The transverse momentum of primary hadrons is assumed given by Gaussian distributions in p_x and p_y separately, with $\langle p_T^2 \rangle = 2\sigma^2$. The symmetric fragmentation function, expressed in the fraction z of remaining energy-momentum that a particle takes, is given by

$$f(z) = \frac{1}{z}(1-z)^a \exp\left(-\frac{b\, m_T^2}{z}\right) \qquad (21)$$

with m_T the transverse mass of the hadron. The two parameters a and b are strongly correlated, e.g. in terms of the mean particle multiplicity obtained. If b is increased or a decreased, the mean multiplicity will decrease. With second order matrix elements and y = 0.02, i.e. $m_{min} \approx 4.5$ GeV, one obtains $\sigma \approx 0.40$ GeV, $a \approx 1$ and $b \approx 0.7$ GeV^{-2}. For parton showers with $\Lambda = 0.4$ GeV and $m_{min} = 1$ GeV, these values are changed to $\sigma \approx 0.35$ GeV, $a \approx 0.5$ and $b \approx 0.9$ GeV^{-2}, i.e. $\langle p_T \rangle$ has to be decreased and f(z) made harder when more gluons are simulated explicitly.

3 Present Phenomenology

Before presenting Monte Carlo results, reasonable numerical values of Λ and m_{min} have to be determined from experimental data. The first one is the most fundamental, namely Λ. If not explicitely given, $\Lambda = 0.4$ GeV is used throughout. Secondly, one has to determine where to stop the perturbative evolution and start with soft physics, i.e. to hadronize. The validity of the perturbative approach becomes increasingly worse as α_s becomes larger, as it does with decreasing argument. The maximum value of α_s is $\alpha_s(m_{min}^2/4)$; with $m_{min} = 1$ GeV and 5 flavours this corresponds to an effective coupling constant $\alpha_s/\pi \approx 1.17$. With an ideal fragmentation scheme and with a perfect fitting between perturbative and nonperturbative physics, results should be insensitive to the precise value chosen for m_{min}. For the following investigations, $m_{min} = 1$ GeV is used, and the sensitivity to m_{min} is investigated in section 3.1.

The aim in section 3.1 is to fix Λ and m_{min} and to compare with some recent high statistics e^+e^- event studies. Section 3.2 contains a thorough investigation of the string effect.

3.1 Standard Event Measures

In section 2.3 is dicussed some of the issues appearing when the complete model, parton showers and a hadronization model, is to be compared with experimentally measured distributions. Whenever a certain set of parton shower parameters is used (Λ and m_{min}) in the following, the parameters of the fragmentation model (a, b and σ) have been retuned to agree with the charged multiplicity distribution and an average p_T. In an earlier paper [2] we investigated some of the features of the model compared to second order matrix elements and, more specifically, we showed that a $\Lambda = 0.4$ GeV and a $m_{min} = 1$ GeV gives a satisfactory agreement with e^+e^- data. The value of Λ is determined by a fit to a three-jet sensitive measure such as the rate of three-clusters. With Λ fixed the effective cutoff mass, m_{min}, determines the remaining rate of pure $q\bar{q}$ events on the parton level. The thrust (T) distribution, at T close to 1, may be used to determine m_{min}. Another

possibility [2,18] is to look at the energy-energy correlation asymmetry distribution at small angles.

We shall not repeat the discussion in [2] but instead use another measure to show that the chosen Λ and m_{min} give a sensible agreement with data and thus justify their use in the following investigations. This will also indicate the sensitivity to the chosen parameters. Consider the sphericity (S) distribution. Ideal two-parton events end up with S = 0 and thus, looking at small S, one may decide the rate of such events allowed by data. In Fig. 2 data from Mark II [19] are shown together with model results for m_{min} = 1 GeV and m_{min} = 4 GeV. The two curves correspond to a two-parton probability of 3% and 35% respectively. Evidently the smaller value is preferred by the data. Turning to the determination of Λ, one must examine the tail of larger S, since this is sensitive to the amount of hard bremsstrahlung. In Fig. 3 data as well as model results are shown for three different Λ:s. The m_{min} was increased to 1.5 GeV to allow for an increase of Λ above the default value ($m_{min} > 2\Lambda$ is required so as to keep α_s finite), but this does not affect the results. It is evident that Λ = 0.2 GeV gives too little radiation and Λ = 0.6 GeV too much, with Λ = 0.4 GeV in good agreement with the data. To end this discussion, the n-cluster ratios are given in Table 1 for data and model results, using the abovementioned parameter sets. It is clearly seen that a change of the cutoff mass m_{min} does not alter the global features in this respect, but that a change in Λ does.

It is interesting to investigate what the running α_s means for comparisons with data. A fixed α_s = 0.32 is determined in the same manner as Λ before. For the comparison to be consistent we have included the condition $p_T^2 \approx z(1-z)m^2 > p_{Tmin}^2$ on branchings, but the same conclusions are reached without it. The number of hard three-jet events is fixed to be the same, but differences appear when virtualities decrease during the evolution. For m_{eff} = 1 GeV the maximum values of α_s may differ by a factor of 10 between the fixed α_s and $\alpha_s(p_T^2)$ cases; thus soft and medium soft gluon bremsstrahlung is strongly underestimated in the former one. In Fig. 4 one can clearly see the effect of fixed α_s. In principle, it is possible to decrease m_{eff} and thereby increase the amount of soft gluon radiation (a fixed $\alpha_s(Q^2)$ does not blow up at $Q^2 = \Lambda^2$!). However, this does not help the situation, probably because the extra amount of radiation is too soft to affect the event shape.

It is interesting to note that also data at a fixed CM energy can be used to give evidence for a running α_s. To the best of our knowledge, this possibility has not been exploited before. Furthermore, in the same figure is shown result with $\alpha_s(m^2/4)$, Λ = 0.45 GeV and m_{min} = 1 GeV. The pattern is very similar to the fixed α_s case; the region with S ≈ 0 is overestimated while the region 0.05 < S < 0.15 is underestimated. Thus, data not only favours a running α_s, but more specifically, that the argument p_T^2 is preferrable to m^2. A cautionary word: our studies have been made within the framework of one very specific fragmentation model, the string one, so a definite conclusion should probably be made only if these features can be reproduced e.g. with cluster fragmentation models as well.

The conventional evolution (including $\alpha_s(p_T^2)$) shows very much the same features as the fixed α_s and $\alpha_s(m^2/4)$ cases above, but less pronounced. Thus, data favours a coherent evolution instead of a conventional one, but the differences are not significant when compared with data. Not only the S distribution shows the phenomena discussed, but a number of other distributions as well.

3.2 Coherence and the String Effect

A couple of years ago JADE first observed that in three-jet events, the region between the quark and antiquark was depleted from particles and energy compared to the region between the gluon and the quark or antiquark (whichever most energetic) [9]. Here the least energetic jet was identified with the gluon, which is not always correct, i.e. a 30% experimental effect is the remnant of roughly a factor two in true difference. The phenomena were well described by string fragmentation and first or second order matrix elements, while independent fragmentation did not fit at all. Since then, the MW-model with coherent parton showers and cluster fragmentation was shown also to give this "string" effect [9,10]. The main point is that coherence, i.e. destructive interference among soft gluons, in some approximation gives this effect. A particularly appealing picture is given by the Leningrad group as follows [20]. Start out with a quark, an antiquark and a gluon, all three approximately with the same energy, and let the three hard partons act as antennas that emit soft gluons in a semiclassical pattern. There is then a surplus of radiation in the region between the gluon and the quark or antiquark and a depletion of radiation in the region between the quark and the antiquark, i.e. opposite to the gluon direction. Furthermore, if a term

proportional to $1/N_c$ is dropped, two terms remain. Each of these can be connected with a two-jet radiation pattern, from qg or $\bar{q}g$, boosted from the qg or $\bar{q}g$ rest frame into the overall $q\bar{q}g$ CM frame. It is then clear that the angular region between the q and $\bar{q}$ quarks is depleted of particles, since this region is opposite to the directions of the boosts for both two-jet configurations, qg and $\bar{q}g$. This scenario literally repeats the explanation given in string fragmentation, so that the picture of perturbative semi-classical gluon bremsstrahlung and nonperturbative string fragmentation here approach each other.

If string fragmentation is accepted as a nonperturbative implementation of coherence, then certainly the string effect proves that coherence effects are important at present energies. One may take a somewhat more narrow point of view, however, and ask whether there is a necessity for coherence on the perturbative level, as opposed to the fragmentation level. Part of the answer is already known: if the parton shower cutoff is chosen so large that the fraction of events with four or more partons is small, there is no difference between coherent and non-coherent parton showers (or matrix elements for that matter), and string fragmentation is enough to explain the data. Such a large cutoff would be in contradiction with other data, as pointed out above, so there is still the possibility that additional emission in a non-coherent scheme could make the string effect go away. This belief has been given some support by the experimental comparisons [10] between the Gottschalk [6] and the MW programs [8]. Both of these are based on cluster fragmentation, the former without and the latter with coherence, the former does not and the latter does exhibit the string effect. This may be misleading, for two reasons. Firstly, the issue of coherence is not the only way in which the two models differ, specifically the cluster fragmentation schemes used are quite distinct. Secondly, cluster and string fragmentation are notably different, in that the former assume isotropic decay in the rest frame of a cluster, whereas the latter imply particle production along the string direction, i.e. transversely to the boost direction for any given string piece. The probability that a particle will end up in an angular region opposite to the boost direction is therefore smaller with string than with cluster fragmentation.

In Table 2 is shown the ratios between N_{13} and N_{12}, where N_{jk} is the integrated particle or energy flow in the region $0.3 < \theta/\theta_{jk} < 0.7$, with θ_{jk} the angle in the event plane between jet j and k, calculated independently for each event. Three-jet events are found with cuts on the eigenvalues of the

sphericity tensor ($Q_1 > Q_2 > Q_3$, $Q_2-Q_3 > 0.07$, $Q_3 > 0.06$). Errors given for the MC data are statistical only. There is a cleaar indication, both from experimental data and from MC data, that the effect increase with increasing $m_T = (m^2 + p_{out}^2)^{1/2}$. Since in the string picture, and even in the semiclassical model discussed above (at least in the $1/N_c$ approximation), the string effect may be viewed as a boost effect, it is evident that particles with larger m_T are affected most. Furthermore, the string effect is not very sensitive to the finer details of the partonic configuration, as clearly seen from the numbers in the table. The gross features of the configurations are already selected by the cuts on the sphericity tensor. Surprisingly, the coherence condition does not add a significant part to the effect, compare line no. 3, without coherence and no. 4, which has coherence included. As a sort of normalization we may regard no. 5 with second order matrix elements, which adds at most one extra parton to the three major ones. The solution of this appearent paradox is a natural consequence of string dynamics and can be explained as follows. Both hard quarks and the hard gluon radiates soft gluons; in the conventional case all three radiate approximately independently and symmetrically (both sides in the event plane of the hard partons are equally populated) but in the coherent case the soft radiation is predominantly in the region between qg and $\bar{q}g$. Now, the question is what happens to soft quanta in the wrong angular region, that between the quarks. In a naive model where partons turns into hadrons independently, final state particles would also appear in the wrong region. But in the string fragmentation scheme the situation is modified by the string motion; soft gluons with low momenta cannot stretch the string far away in the "wrong" direction before it stops, and eventually a large part of the string is moving in the "right" direction before it breaks up into hadrons [21]. The scenario in the coherent case may be viewed as an attempt to form a string from soft partons. Partons are predominantly emitted in the directions where the string already would have been if only the three hard partons ($q\bar{q}g$) were used for the string drawing.

In the last three lines in Table 2 we show results using events which are not hadronized. The modification from the matrix element correction is not significant but adding coherence increase the ratios by approximately 10%, at least if one disregard the second column where statistics are poorer. Our conclusions are the following. Compared to matrix elements, parton showers gives a more complicated string topology, which seems to make the string effect somewhat smaller. Coherence adds a significant part to the phenomena at parton level, but on the hadron level this part is washed out because of the

dynamics of the string. The string effect therefore is not a proof of the need for coherence in the perturbative treatment. This is no way intended as an attack on the concept of coherence as such, just as a plea for a more balanced view in the interpretation of data.

4 Investigations at Larger Energies

We start in section 4.1 with multiplicity distributions, continue in section 4.2 with the connection between parton and charged multiplicity. Section 4.3 deals with x and y distributions, section 4.4 with energy-energy correlations and 4.5 with angular ordering and a possible experimental verification of coherence effects.

4.1 Parton Multiplicity Distributions

The number of produced partons is of great interest because, as we will see later on, parton and hadron multiplicities are interrelated. For a first study, only gluon jet evolution through branchings $g \to gg$ is included, so as to exclude any dependence on quark masses etc.; this will give the main features anyway. Average parton multiplicities are plotted in Fig. 5 for four different cases and energies from 10 GeV to 10 TeV. The first case is with the local z definition, massive daughters, $\alpha_s(m^2/4)$ and without including coherence. A slow multiplicity development is obtained, giving less than 35 gluons on the average at 10 TeV. Changing to the global z definition, there are two effects which increase the multiplicity considerably. The β factor in eq. (10) increases, since it is now calculated in the total CM frame, and the vanishing of daughter masses results in a larger z range and phase space for emission. A further change of the argument in α_s from $m^2/4$ to $p_T^2 = z(1-z)m^2$ has two consequences. Firstly, since $m^2/4 > z(1-z)m^2$ the coupling is increased, secondly, there is a further constraint $z(1-z)m^2 > m_{eff}^2$ which decreases the available phase space. These two effects tend to cancel in the multiplicity. When coherence is added, the constraint in eq. (20) reduces the available phase space further, and the multiplicity growth becomes more moderate. As a last comparison, an analytic equation for the multiplicity growth in coherent showers [22] has been normalized to our coherent case at 10 GeV. The analytic formula predicts a larger increase than the comparable MC data; approximately a factor of 1.5 over four orders of magnitude in jet energy. In summary, the parton multiplicity is very sensitive to the treatment of kinematics, and may

differ by almost a factor of 10 at 10 TeV for the cases studied. The dramatic change in multiplicity growth between different z choices for the conventional case is not at all that large for the coherent case (not shown in the Figure). Thus, adding coherence makes the interpretation of the z variable less critical, at least in this respect. The global choice of z, and the way kinematics is treated in this case, comes closest to the analytic formula derived from QCD.

In theoretical papers, it is often remarked that the coherent multiplicity growth is smaller than the conventional one. This is certainly true, if one thinks in terms of starting out with a given conventional model, and then introduce angular ordering as an extra constraint. The range of possible conventional models is very large, however, and many of these have a multiplicity growth that is slower than given by the standard analytical formula for the coherent case, let alone for the conventional one. (Many of these differences may be of subasymptotic nature, i.e. the expected behaviour is recovered at very high energies, when $\alpha_s(Q^2)$ is truly small number.) One example of a conventional model with slow growth is given here, another one is the Kajantie-Pietarinen algorithm [5] as implemented in JETSET version 6.2 [13], a third one the algorithm used in ISAJET [23]. The parton multiplicity growth is therefore not a good criterion for the angular ordering properties of a model.

To give one example of the importance of subasymptotic effects, consider the requirement $m_b + m_c < m_a$ in a branching $a \to bc$, a constraint that is often reduced to $m_b, m_c < m_a$ in analytical calculations. The starting point is given by a previous calculation of the mean parton multiplicity [4,24], valid for the conventional case. The standard evolution equation for the fragmentation function $D(x,m^2)$ can be written as [4,24]

$$\Delta D(x,m^2) = -\frac{\alpha_s}{2\pi}\frac{\Delta m^2}{m^2}\left\{\int_{z_-(m^2)}^{z_+(m^2)} dz\, P(z)\right\} D(x,m^2) +$$

$$+\frac{\alpha_s}{2\pi}\frac{\Delta m^2}{m^2}\int_0^1 dy \int_{z_-(m^2)}^{z_+(m^2)} dz\, P(z)\left\{\delta(x-yz)D(y,m^2) + \delta(x-y(1-z))D(y,m^2)\right\} \qquad (22)$$

with

$$P(z) = C_A \frac{(1-z(1-z))^2}{z(1-z)} \quad . \tag{23}$$

However, the daughters should not be allowed to have the full virtuality of the mother, i.e. they can not be evolved independently. If, for simplicity, we adopt the light-cone definition of z, then $p_T^2 = z(1-z)[m_a^2-m_b^2/z-m_c^2/(1-z)]$ and, in a first approximation, $m_b^2 < zm_a^2$ and $m_c^2 < (1-z)m_a^2$. The requirement $p_T^2 \geqslant 0$ leads to the more stringent conditions $m_b^2 \leqslant \alpha z m_a^2$ and $m_c^2 \leqslant (1-\alpha)(1-z)m_a^2$, where $\alpha = 1/2$ is preferred for symmetry reasons. Insert this in eq. (22), use $\alpha_s(m^2)$, integrate over x to get the total average multiplicity and keep only logarithmic terms in the z integrals. The resulting differential equation is then

$$\frac{d}{d\tau}(\tau\frac{dN(\tau)}{d\tau}) = \frac{C_A}{\pi b} N(\tau-a) - \frac{m_{min}^2}{\Lambda^2} e^{-\tau}\{N(\tau-a) - N(\tau) + \frac{dN(\tau)}{d\tau} - \frac{dN(\tau-a)}{d\tau}\} \tag{24}$$

with $\tau = \ln(m^2/\Lambda^2)$, $a = \ln(1/\alpha) > 0$ and $b = (11N_c)/(12\pi)$. Since we are interested in a solution in the asymptotic domain where τ is big, the term proportional to $e^{-\tau}$ is small and (24) reduces to

$$\frac{d}{d\tau}(\tau\frac{dN(\tau)}{d\tau}) = \frac{C_A}{\pi b} N(\tau-a) \tag{25}$$

which is equivalent to the "standard" differential equation except for the argument on the right hand side. The derivatives on the left hand side are proportional to $N(\tau-a)$ rather than to $N(\tau)$. Since $N(\tau-a) < N(\tau)$ the multiplicity growth will be reduced. Now expand the right hand side for small a and keep only the two first terms. Then the equation is possible to solve and, except for an absolute normalization factor, the solution is

$$N(\tau) \sim \tau^{-\beta/2} I_\beta\{2[\frac{C_A\tau}{\pi b}]^{1/2}\} \tag{26}$$

with $\beta = (aC_A)/(\pi b)$ and I_β the modified Bessel function of order β. Asymptotically, eq. (26) reduces to

$$N(\tau) \sim \tau^{-(\beta+1/2)/2}\exp\{2[\frac{C_A\tau}{\pi b}]^{1/2}\} \tag{27}$$

which, except for the extra β in the first exponent is identical with the one presented in [4,24]. However, β approximately equals 0.76, which significantly changes the behaviour of the first term and of the whole expression. In Fig. 6 the average multiplicities are shown for $\beta = 0$ and $\beta = 11\cdot\ln(2)/12 \approx 0.76$, with a normalization such that they both agree at 10 GeV. Here we find a difference of a factor of 1.5 between the two cases. It is not impossible that

the same kind of factor is responsible for the discrepancy between model results and the analytical expression presented in [22]. This phenomenon is of course also present in the case of a coherent evolution, but here the calculation is not so simple.

4.2 Relation Between Parton and Hadron Multiplicity

The relation between the charged particle multiplicity (which is proportional to the total particle multiplicity) and the parton multiplicity is interesting to investigate; in particular there exist predictions [25] that the mass spectrum of colour singlet clusters is independent of CM energy, which suggest that parton and hadron multiplicities should be proportional to each other at asymptotic energies. In string fragmentation the particle multiplicity is approximately given by (the logarithm of) the string "length" in momentum space, which is not only sensitive to the number of partons and their respective energies but also to the way the string is stretched between the partons. In Fig. 7, the ratio of charged to parton multiplicity is shown for energies from 10 GeV to 10 TeV and for four different cases; local z vs. global z, $\alpha_s(m^2/4)$ vs. $\alpha_s(p_T^2)$ and conventional vs. coherent parton showers in different combinations explained in the figure text. For the lowest energy, bremsstrahlung is not so important and all the four ratios are approximately equal. At asymptotic energies the ratios approach constant values, although different for the different cases. The charged multiplicity growth is sensitive to the choice of evolution scheme; there is a difference by a factor of two at 10 TeV for the most extreme cases. This is still less than the factor of 10 on the parton level. Thus there is a tendency that a higher parton multiplicity growth gives a smaller asymptotic ratio. The dependence on the argument in α_s is transparent, since $\alpha_s(m^2/4)$ and $\alpha_s(p_T^2)$ give approximately the same number of partons; with $\alpha_s(p_T^2)$ the cut $p_T^2 \geqslant m_{eff}^2$ will see to it that string pieces have a minimum length, thus giving a higher particle multiplicity. If a bigger m_{min} is used, e.g. 1.5 GeV instead of 1 GeV, this effect is much more visible since the minimum string length is then increased. Needless to say, the absolute number of partons obtained is very sensitive to the cutoff m_{min} used, while the charged multiplicity is not (due to the infrared stability properties of string fragmentation). With independent fragmentation, as implemented in JETSET 6.3 [13,14], ratios increase continuosly with energy, without levelling off.

One may understand the proportionality between particle and parton multiplicity as follows. Imagine a parton cascade in momentum space, with the string spanned between colour connected final state partons. When the energy is increased the tree will grow, both in parton multiplicity and in string length. There is a universality in the low- to medium-Q^2 part of the shower evolution, however, so that the crown of the tree looks the same for a small tree (low energy) as for a bigger one (high energy). In other words, the average number of partons connected per string length is constant and independent of energy.

4.3 x and Y Distributions

The way the total energy in an event is shared between the produced gluons can give information on the production mechanism. In Fig. 8, the energy ratio $x = 2E/s^{1/2}$ is plotted (in a log scale in x) as $(x/\sigma)(d\sigma/dx)$ for $s^{1/2} = 1$ TeV. This distribution is very dependent on the parton multiplicity, but differences show up even in cases with identical average multiplicities. The first curve is for the local z case with $\alpha_s(m^2/4)$ and coherence excluded; this curve decreases smoothly towards zero for $x \to 1$ and $x \to 0.001$ with a broad peak at $x \approx 0.04$. Moving to the global z case, the multiplicity is increased substantially, and the distribution acquires a bump at very small x-values while the tail for $x \to 1$ is reduced. The shift towards smaller values of x is related to the increased multiplicity, but a further change from $\alpha_s(m^2/4)$ to $\alpha_s(p_T^2)$ alters the distribution without changing the multiplicity. The region close to $x = 1$ is less populated, the one at small x is depleted and the peak at $x \approx 0.02$ is not so wide. These differences are caused by the condition $p_T^2 = z(1-z)m^2 \geq m_{eff}^2$: the cut in z gives branchings with less difference between the daughter energies. The fact that $\alpha_s(p_T^2)$ is peaked at small p_T:s does not seem to fully compensate for this effect. Adding the coherence condition on the evolution reduces the multiplicity and shifts the x distribution towards bigger x values. The region at small x has been further depleted, characteristic for the destructive interference among soft gluons, and the peak is shifted to $x \approx 0.03$. In Fig. 9 the same distribution is shown for the MW model [8] together with two curves for our coherent case; one with the default value of m_{min} (1 GeV) and the other with $m_{min} = 0.84$ GeV. This clearly illustrates the infrared sensitivity of the x distribution. With $m_{min} = 0.84$ GeV and $\Lambda = 0.4$ GeV our results come very close to the MW ones where $m_{min} = 1.4$ GeV and $\Lambda = 0.2$ GeV have been used (the difference between these two setup of parameters is consistent with what is needed to describe PETRA/PEP data

with the two respective models).
As seen in section 4.2, the large differences in parton multiplicities are significantly reduced by fragmentation effects, but still partly survive. The same can not be said of the x spectra: at 1 TeV the differences are dominated by the differences in particle multiplicities, and the depletion at small x in the coherent case is washed out by the fragmentation.

The study of rapidity distributions is standard both in hadron and in e^+e^- physics. Reminiscences of coherence effects are expected to show up: the depletion of the region of low x should be repeated in the rapidity spectrum. The pattern is not so simple, however. Firstly, a physical axis of the final state partons has to be specified. Here the linear sphericity axis will be used, rather than some axis intrinsic to the branching process (cf. comments in [8]). Secondly, one must remember that the central rapidity region is populated not only by soft gluons but also by wide-angle gluons at higher x values. For comparison, distributions are again shown at 1 TeV energy, Fig. 10. As before, start with the local case, with $\alpha_s(m^2/4)$ and coherence excluded. In the central rapidity region up to $|Y| \approx 1.5$ the distribution is essentially flat and ends in a tail at $|Y| \approx 8$. Events where the two original gluons have not radiated and hence have an undefined rapidity are disregarded. The average multiplicity is increased when the global z definition is used and, as a consequence, the average x value is decreased. The peak at very small x is reflected in a corresponding peak at $Y = 0$; the former plateau has disappeared and the tail to large rapidities has also decreased somewhat. Using p_T^2 instead of $m^2/4$ as argument in α_s decreases the amount of very soft and very hard gluons, see above. The peak at $Y = 0$ still remains, but a small bump at $|Y| \approx 2.5$ shows up as a consequence of the abovementioned argument. The tail is also reduced further for the same reasons. Finally, adding coherence depletes the region at small x and a dip at $Y = 0$ appears in the rapidity distribution. The effect is not caused by the depletion at small x solely, since a corresponding dip is absent in the local z case, which has a similar x distribution. In the coherent case, because of angular ordering, the gluons has more difficulty to emerge at large angles from the initial parton axis and then end up at $Y = 0$ with a moderate x value. The dip thus appears to be a true coherence effect. The phenomenon remains when quarks are included in the process.

When events are hadronized, but the old linear sphericity axis of the partons is used, no dip appears, either in the conventional case or in the coherent one. Only when the hadronic final state is used to define the linear

sphericity axis a dip shows up, but now in both cases. This shows that the question of a dip or not is extremely sensitive to the axis used for the definition of rapidity. An even larger dip is obtained with the thrust measure. Here a variation of the trial jet axis by an amount $\delta\theta$ gives a contribution to thrust proportional to $\delta\theta$ for particles around $\theta = 90^0$ w.r.t. the axis, but proportional to $(\delta\theta)^2$ for $\theta \approx 0^0$. In other words, while the gross direction of the thrust axis is determined by high-momentum particles, the "fine tuning" of this direction tends to deplete the region close to 90^0, i.e. $Y = 0$. There is also another aspect to the question of rapidity dips in the hadronic state: even for three-parton configurations, the string effect contributes by boosting particles away from the $Y \approx 0$ (and $x \approx 0$) region, while no corresponding depletion is obtained with independent fragmentation. This explains why dips can be obtained also without any need for coherence in the parton shower evolution. However, at 1 TeV the dip is slightly more pronounced in the conventional case than in the coherent one, Fig. 11. Since the opposite situation is observed at the parton level this change was not expected. The phenomenon is apperently an effect of string fragmentation and may be understood as follows. One of the string pieces spanning the region at $Y = 0$ is the one that connects the first gluon emitted on either side. These gluons are normally emitted at larger angles, i.e. the string may be significantly tilted with respect to the jet axis, and therefore the particle production is more squeezed together at central rapidities. One such string piece is to be found in each event but in the coherent case, where the average number of string pieces (both in total and those passing $Y = 0$) is smaller, that one piece obtaines a higher relative weight.

4.4 Energy-Energy Correlation

It has been proposed that one place where coherence effects show up is in the energy-energy correlation function (EEC) [26], in the region of angles θ close to 180^0. The EEC is proportional to the number of parton pairs forming a relative opening angle θ, weighted by the product of the respective parton energies. In a previous paper [27] it was shown that a conventional algorithm differed by almost an order of magnitude from the analytic QCD prediction at angles $\theta \approx 180^0$ and a CM energy of 6 TeV. The coherent scheme, on the other hand, came remarkably close to the analytic prediction. Both algorithms were implemented in JETSET 6.2, with $\Lambda = 0.25$ GeV. However, the implementations used not only differ as to angular ordering, but also in the choice of z variables etc.. Here we will test the effect of coherence solely, without any

extra differences. For convenience, the choice of $\Lambda = 0.25$ GeV and CM energy 6 TeV is retained.

In Fig. 12, is compared analytical predictions [28], conventional evolution with local and global z definition, and the coherent case with global z. As shown in [27] and reconfirmed here, the dependence on the argument in α_s is small, both for conventional and coherent evolution; all the results above are for $\alpha_s(p_T^2)$. The agreement between the coherent and the analytical curve is remarkably good, considering that they are based on quite different approaches to QCD theory, and that both are extrapolations over two orders of magnitude in CM energy.

Compared to the results of [27], the difference between conventional and coherent evolution has shrunk significantly. Taking the value at $1 + \cos\theta \approx 10^{-6}$ as a simple measure, this was roughly 10000 with the old conventional algorithm, is 4500 with the present conventional with local z, 2300 with global z and 1800 with the present coherent one. This does not help much as far as practical applications go, since initial state photon radiation is enough to mess up what should be meant by a back-to-back pair. On the other hand, the region of very small angles is experimentally well defined, but the differences that actually may be found there between conventional and coherent models are completely wiped out by fragmentation effects.

4.5 Angular Ordering

The angular ordering condition, eq. (20), is motivated only in the asymptotic domain, where daughter virtualities are much smaller than the mother one. Therefore it is interesting to know how well the condition $\theta_3 \leqslant \theta_1$ is fulfilled in reality. Ratios of consecutive opening angles in 100 GeV events are plotted in Fig. 13; the results at 1 TeV are similar. Here p_T^2 is used consistently as argument in α_s. In the local z case, without coherence, the percentage of nonordered branchings ($\theta_3/\theta_1 > 1$) is 35%. Further, there is a narrow peak at 0.1-0.2. When coherence is introduced in the branching process one must remember that, for the local z definition, opening angles are approximately ordered only in the rest frame of the grandmother. The boost to the total CM frame may therefore alter the angular ordering. The number of nonordered branches is decreased to 20% and the peak remains. In the global z, noncoherent case, there is a large number of nonordered consecutive angles, approximately 50%. The distribution is no longer peaked in the first bin,

instead a plateau for $0 < \theta_3/\theta_1 < 0.5$ shows up. At 1 TeV, a sharp peak appears at very small ratios, less than 0.1, in this case. This peak is built up by events where an energetic parton with a small mass has radiated a soft gluon at a large opening angle, thereafter the more energetic daughter, which has a very small mass, is split fairly symmetrically, i.e. with a small p_T. The reason for a symmetrical split is that, for small masses, that is the only way the condition $p_T^2 \approx z(1-z)m^2 > \Lambda^2$ can be fulfilled.

Finally, consider the global z with coherence condition included. Here eq. (19) is evaluated in the CM frame, and the fraction of nonordered angles drops to 12%. It is thus only with the global z definition that the angular ordering condition works as expected. Partons, which in principle have a large phase space for nonordered branchings, will instead tend to end up in a broad peak at around $\theta_3/\theta_1 \approx 0.5$. The distribution is decreasing monotonically at small angles, without any narrow peaks close to the origin.

One very direct test of coherence would be if angular ordering could be studied, based on the properties of the hadronic final state. Since partons can not be observed directly, it is first necessary to use some cluster algorithm, which groups the particles into jets. (In order to remove some background from semileptonic decays of charm and bottom, jets where leptons carry more than half the energy are removed from further consideration. Top production is also not included in the following, since the top mass is unknown. Contamination from top events may be important, but probably cuts can be used to reduce it significantly.) These jets should hopefully mirror the underlying partonic configuration. The likely event history may now be reconstructed backwards, step by step as follows.

- Find the two jets which has least invariant mass.
- Add these jets to get their mother jet.
- If more than two jets left, loop back.

From the reconstructed event history, the ratio of consecutive angles may then be found. In principle, there is one nontrivial parameter in the problem (d_{join} in LUCLUS, see [13]), which is related to the "jet resolution power" used. If this is set at too low a value, the fragmentation products of one single parton (or, more properly, of the string pieces close to a single parton) may be split up into several jets. Then spurious opening angles will be reconstructed, that are not a part of the cascade but related to fragmentation phenomena. If the jet resolution is put too high, on the other hand, the number of reconstructed jets is too small, and the region of small opening angles can not be studied at all. As it turns out, results are not

that sensitive to the choice of jet resolution power; in the following d_{join} = 3 GeV has been used. Further, only the global z case with $\alpha_s(p_T^2)$ is discussed here. For two consecutive branchings, $1 \to 2 + 3$ with opening angle θ_1 and $3 \to 4 + 5$ with θ_3, the ratio $r = \theta_3/\theta_1$ is defined. In order to improve the discriminating power, the dependence of this ratio on the mass m_3 (= m^*) will also be studied.

It is useful to define a measure gauging the shape of the r distribution. Perhaps the most natural choice would have been to use the fraction of nonordered opening angles, as in the partonic case. Unfortuntely the tail of large ratios r is contaminated with irrelevant combinations. Instead we have chosen to define a ratio $n(1.4 < r < 2.0)/n(0.0 < r < 0.6)$, i.e. the number of angular sets that are clearly nonordered, excluding the suspect tail, divided by the number of sets that are clearly ordered. The results are not sensitive to the exact limits used. Results at 200 GeV are plotted in Fig. 14 a. For large masses (m^*), above 26 GeV, the conventional and coherent algorithm coincide. This may be used as a common normalization, from which the "signal" may be seen. At small masses, below 16 GeV, the conventional case gives an increased amount of nonordered opening angles, and the measure increases more rapidly than for the coherent case. Where statistics is best, between 12 and 16 GeV, also the difference is largest, about a factor of two. At 94 GeV (typical SLC/LEP I energy), the task is significantly more difficult. These results are shown in Fig. 14 b. The basic features are the same, but the factor two separation now has decreased to 1.5. It is then more difficult to say how much could be made out of signal, considering possible model dependent variations. On the other hand, it should be possible to find a set of improved cuts and a better tuned history reconstruction, so that the significance of the separation is increased.

5 Onia Physics - Quark vs. Gluon Jets

Quarkonium resonances, like J/Ψ or Υ, have a significant probability to decay into gluonic states. For 1^{--} resonances these may be of the ggg or ggγ kind. Therefore a completely different event structure is expected on resonance, compared to the underlying continuum $q\bar{q}$ events. In terms of global event measures like, say, charged multiplicity or sphericity, these differences are indeed observed. However, the energies involved at Υ are far too small to allow a seperation into three jets. The study of a toponium resonance could here provide interesting information. The data from PETRA tell us the

resonance mass must be larger than 47.2 GeV, while weak decays of the individual top quarks will start to dominate if the mass is much above that. The scenario of a 50 GeV resonance will therefore be studied in some detail.

When parton showers are attached to the basic three-body decay of the toponium resonance, special problems are encountered: how should kinematics be reconstructed from three original massless partons to three massive ones, without too severe a violation of the original configuration? Furthermore, the maximum allowed virtuality of each parton is somewhat arbitrary. We have here chosen a simple scheme, which probably contains the main features, as follows. The energy of each parton in the CM frame is assumed conserved. Consequently the maximum allowed virtuality of a parton is set equal to its energy. Usually the angles between the partons, as well as the three-momenta, are changed when masses are introduced. If the triplet of gluon masses is such that the kinematics reconstruction becomes impossible, the parton with largest m/E (= $m_{present}/m_{max}$, see sect. 2.2) is evolved further. The overall orientation of the event contains three independent degrees of freedom (Euler angles). Two of them are fixed by the conservation of the event plane, while the third is somewhat arbitrary fixed by the conservation of the direction of one three-momentum.

Contrary to the case for continuum production, we have not tried to match up with the matrix elements of next order, $O(\alpha_s^4)$. These are known [29], but are too complex to be worth the effort here. Instead the first branching on each leg is decoupled from the original gluon configuration, and coherence is only included in the subsequent branchings.

Toponium events are expected to be different from continuum events. In particular, they are expected to be more spherical, since the decay matrix element $t\bar{t} \rightarrow ggg$ produces an essentially uniform distribution in the three-body phase space, and since gluons radiate more than quarks. Further, in the string fragmentation scheme, the string is stretched in a triangle between the three gluons and, since the multiplicity is dependent on the string length, a larger multiplicity than in the continuum is expected already for that reason.

The average charged multiplicity obtained for continuum events at 50 GeV is 16.5, for gluonium ones 26.1. Apart from experimental uncertainties, a cut at 21 would separate an equal mixture of the two event types with only 20% misidentification (the actual mixture would depend on the beam energy spread of the machine used). Thrust, sphericity, aplanarity and other distributions

all show how little two-jetlike gluonium events are. In Fig. 15 the aplanarity (A) distribution is shown for three cases; continuum events, gluonium without parton showers and gluonium with parton showers. On the parton level, the continuum events have a contribution to A from the parton shower evolution, while onia decays into three gluons have not. Still A is bigger in the latter case because of fragmentation effects, essentially the larger multiplicity. The introduction of bremsstrahlung in onia decays gives a significant contribution to A, both on the parton and on the hadron level. If a cut A = 0.032 is introduced, it is possible to identify gluonium and continuum events with approximately 18% misidentified events. Simultaneous cuts on several distributions may increase the significance, but the correlation between different measures is a limiting factor.

If toponium is found, it is possible to investigate the special features of gluon jets relative to quark jets with a much safer identification than possible before. One test is jet masses, which are believed to be larger for gluon jets because of their larger colour charge. In Table 3, average jet masses are shown, at the parton and the hadron level, for different initial configurations and energies. A cluster algorithm is used to reconstruct exactly two jets in the continuum or in $gg\gamma$ events and three jets in ggg ones. On gluonium (ggg) as well as radiative events ($gg\gamma$), cuts on the angles between jets are imposed ($90^\circ < \theta_{ij} < 150^\circ$) to ensure that the jet energies are approximately equal. In the two first lines, $q\bar{q}$ events and gg ones (e.g. obtained from "tagged" $gg\gamma$ events by a boost along the γ) are compared at 29 GeV, free from the special kinematics ambiguities in ggg. A difference is readily visible, but the factor 9/4 in gluon to quark colour charge is not fully realized. The increase in jet mass from fragmentation is somewhat larger for gluons, as expected from the larger multiplicity. In the third line, results for $gg\gamma$ events at 50 GeV are presented; because of the angular cuts above, the two-gluon system has the typical mass 29 GeV, so that almost the same figures are obtained as for gg above. In the non-radiative onia decays (ggg), jet masses are decreased compared to the radiative ones, for two reasons. Firstly, the extra kinematics constraints due to having three partons somewhat reduce the amount of evolution. Secondly, with three jet axis to be determined, there is an increased amount of large-angle emission that can be assigned to another jet than the one it was emitted from. In reality, jet masses will therefore not give a good separation between quark and gluon jets.

The string effect, see sect. 3.2, is a consequence of the topology of the string. In onia decays, the string is closed (neglecting quark pair production) and the regions between the three jets are on an equal footing. Not so for three-jet continuum events, where there is no string between the quark and the antiquark. In Fig. 16 the particle flows for the two cases at 50 GeV are compared, using the same event cuts as before. Indeed, the region between jet 1 and jet 2 is not that depleted in the onia case. The increased jet width is also readily visible. Therefore, the depletion observed between the quark and the antiquark jet in $q\bar{q}g$ events should have no correspondence in ggg ones, apart from minor geometrical effects.

As in Table 2, a ratio may be defined between the central region between jets 1 and 3 and between jets 1 and 2. For the particle multiplicity, the numbers are 1.31 for continuum events and 1.06 for onium ones, with similar differences for the other measures. An experimental observation of this pattern would be an excellent confirmation of the difference in colour structure between quarks and gluons.

6 Conclusions

Our aim has been to construct an algorithm, based on the AP evolution equations, where it is possible to switch on and off coherence without introducing any extra differences in the algorithm. Furthermore, kinematical and dynamical variables are expressed in terms of Lorentz invariants, and the three-jet matrix element is used as a guideline for the first branchings. Several other options are also included, allowing different treatments of the kinematics in branchings and the use either of $\alpha_s(m^2/4)$ or $\alpha_s(p_T^2)$. Thus we have at our disposal a laboratory for the study of the importance of several features of perturbative QCD.

In a paper by Odorico [30], it is suggested that coherence phenomena are phenomenologically irrelevant at present energies. We do not entirely agree with the argumentation in that paper, but tend to arrive at similar conclusions. More specifically, if a string fragmentation scheme is used, equally good descriptions of data can be obtained either angular ordering is imposed or not. This applies also for the well-known string effect: the differences present on the parton level are drowned by the effects of fragmentation. Whether similar conclusions would be obtained with other fragmentation schemes is not known. In some sense, the string fragmentation

scheme by itself includes several features of the colour coherence phenomenology [20] so that also non-coherent parton shower evolution will work, at least at present energies. Surprisingly, the evidence for a running α_s, with argument p_T^2 rather than m^2, may be more convincing than that for angular ordering.

At higher energies, the most direct test for angular ordering is the slower increase in multiplicity. On the parton level, the difference can be a factor of ten at 10 TeV, which is reduced to a more modest factor of two when hadronization is included. But the multiplicity growth is sensitive to a number of features of a model, which makes it difficult to separate the influence of coherence solely on this effect. For example, the exact interpretation of z splitting variable and related kinematics is very important for non-coherent parton shower programs, however, so that the range of possible algorithms stretches to those with a multiplicity growth as given by the analytical formula for the coherent case. Equally discouraging conclusions are reached for a number of other measures. The depletion of partons at small x from coherence effects is visible enough, and distinct from what is obtained with a wide range of non-coherent algorithms, but the difference does not survive fragmentation. Neither does a related dip at rapidity Y = 0.

The list could be made longer, but the conclusion is clear enough: for any one single observable at any given energy, it seems possible to find a conventional algorithm that gives pretty much the same results as the coherent one, once fragmentation effects have been included. It is not the same conventional algorithm that gives agreement with the coherent one for all the distributions at the same time, however, neither does agreement at any one energy necessarily guarantee agreement over a wide range of energies for a fixed setup of parameters. As a first suggestion towards different and more direct tests of coherence, we outline a method for actually studying the extent to which subsequent angles of emission are ordered. The situation is therefore not desperate - we are confident that continued experimental analyses could gradually shrink the range of allowed models. This will require a more sophisticated thinking and a more careful separation between perturbative and nonperturbative physics.

References

1. A. Ali, J. G. Körner, Z. Kunszt, E. Pietarinen, G. Kramer, G. Schierholz, J. Willrodt, Nucl. Phys. B167 (1980) 454
   K. J. F. Gaemers, J. A. M. Vermaseren, Z. Physik C7 (1980) 81
   R. K. Ellis, D. A. Ross, A. E. Terrano, Nucl. Phys. B178 (1981) 421
   J. A. M. Vermaseren, K. J. F. Gaemers, S. J. Oldham, Nucl. Phys. B187 (1981) 301
   K. Fabricius, G. Kramer, G. Schierholz, I. Schmitt, Z. Physik C11 (1982) 315
   Z. Kunszt, Phys. Lett. 99B (1981) 429
   F. Gutbrod, G. Kramer, G. Schierholz, Z. Physik C21 (1984) 235
   T. D. Gottschalk, M. P. Shatz, Phys. Lett. 150B (1985) 451

2. M. Bengtsson, T. Sjöstrand, LU TP 86-18 (1986)

3. G. C. Fox, S. Wolfram, Nucl. Phys. B168 (1980) 285
   C.-H. Lai, J. L. Petersen, T. F. Walsh, Nucl. Phys. B173 (1980) 244
   R. Kirschner, S. Ritter, Physica Scripta 23 (1981) 763

4. R. Odorico, Nucl. Phys. B172 (1980) 157

5. K. Kajantie, E. Pietarinen, Phys. Lett. 93B (1980) 269

6. T. D. Gottschalk, Nucl. Phys. B214 (1983) 201

7. A. H. Mueller, Phys. Lett. 104B (1981) 161
   B. I. Ermolaev, V. S. Fadin, JETP Lett. 33 (1981) 269
   A. Bassetto, M. Ciafaloni, G. Marchesini, Phys. Rep. 100 (1983) 201

8. G. Marchesini, B. R. Webber, Nucl. Phys. B238 (1984) 1
   B. R. Webber, Nucl. Phys. B238 (1984) 492

9. JADE Collaboration, W. Bartel et al., Phys. Lett. 101B (1981) 129, ibid. 134B (1984) 275, ibid. 157B (1985) 340

10. TPC Collaboration, H. Aihara et al., Z. Physik C28 (1985) 31

11. TASSO Collaboration, M. Althoff et al., Z. Physik C29 (1985) 29
    Mark II Collaboration, P. D. Sheldon et al., Phys. Rev. Lett. 57 (1986)

1398

12. B. Andersson, G. Gustafson, G. Ingelman, T. Sjöstrand, Phys. Rep. 97 (1983) 33

13. T. Sjöstrand, Computer Phys. Comm. 39 (1986) 347

14. T. Sjöstrand, M. Bengtsson, LU TP 86-22 (1986)

15. B. R. Webber, Cambridge preprint 86/3 (1986), to appear in Ann. Rev. Nucl. Phys.

16. G. Altarelli, G. Parisi, Nucl. Phys. B126 (1977) 298

17. D. Amati, A. Bassetto, M. Ciafaloni, G. Marchesini, G. Veneziano, Nucl. Phys. B173 (1980) 429
    G. Curci, W. Furmanski, R. Petronzio, Nucl. Phys. B175 (1980) 27

18. JADE Collaboration, W. Bartel et al., Z. Physik C25 (1984) 231

19. A. Petersen, in the proceedings of the Mark II 1986 workshop at Granlibakken, SLAC-Report-306

20. Ya. I. Azimov, Yu. L. Dokshitzer, V. A. Khoze, S. I. Troyan, Phys. Lett. 165B (1985) 147, Leningrad preprint 1051 (1985)

21. T. Sjöstrand, Phys. Lett. 142B (1984) 420, Nucl. Phys. B248 (1984) 469

22. A. Bassetto, M. Ciafaloni, G. Marchesini, A. H. Mueller, Nucl. Phys. B207 (1982) 189
    J. B. Gaffney, A. H. Mueller, Nucl. Phys. B250 (1985) 109

23. F. E. Paige, S. D. Protopopescu, in Observable Standard Model Physics at the SSC: Monte Carlo Simulation and Detector Capabilities, eds. H.-U. Bengtsson, C. Buchanan, T. Gottschalk, A. Soni (World Scientific, Singapore, 1986) p. 213

24. A. Bassetto, M. Ciafaloni, G. Marchesini, Nucl. Phys. B163 (1980) 477

25. D. Amati, G. Veneziano, Phys. Lett. 83B (1979) 87

26. C. Basham, L. Brown, S. Ellis, S. Love, Phys. Rev. Lett. 41 (1978) 1585

27. T. Sjöstrand, D. E. Soper, in Supercollider Physics, ed. D. E. Soper (World Scientific, Singapore, 1986), p. 283

28. J. C. Collins, D. E. Soper, Nucl. Phys. B193 (1981) 381, ibid. B213 (1983) 545, ibid. B194 (1982) 445, ibid. B197 (1982) 446
J. Kodaira, L. Trentadue, Phys. Lett. 112B (1982) 66
J. C. Collins, D. E. Soper, "The Two Particle Inclusive Cross Section in e^+e^- Annihilation at PETRA, PEP and LEP Energies, "Argonne preprint anl-hep-pr-85

29. K. Koller, K. H. Streng, T. F. Walsh, P. M. Zerwas, Nucl. Phys. B193 (1982) 61, ibid. B206 (1982) 273

30. R. Odorico, Z. Physik C30 (1986) 257

Table 1

The n-cluster rate for Mark II data [19] and model results, with Λ and m_{min} values as given in the table.

		2-cluster	3-cluster	4-cluster
data		0.652 ± 0.025	0.311 ± 0.018	0.037 ± 0.012
Λ (GeV)	m_{min} (GeV)			
0.4	1	0.667 ± 0.007	0.311 ± 0.005	0.022 ± 0.002
0.4	4	0.661 ± 0.009	0.315 ± 0.007	0.024 ± 0.003
0.2	1.5	0.730 ± 0.007	0.253 ± 0.005	0.016 ± 0.002
0.4	1.5	0.654 ± 0.009	0.322 ± 0.007	0.024 ± 0.003
0.6	1.5	0.625 ± 0.008	0.345 ± 0.006	0.030 ± 0.002

Table 2

The ratio of the number of particles in the angular region $0.3 < \theta_{ij}/\theta_{jk} < 0.7$ between jets 1 and 3 to the corresponding number between jets 1 and 2. The angle θ_{jk} is between jets j and k and θ_{ij} is the angle between particle i and jet j. Line no. 1 is with the local z, $\alpha_s(m^2/4)$ and no coherence, no. 2 as no. 1 but with the global z, in no. 3 $\alpha_s(p_T^2)$ is introduced, in no. 4 coherence is included, in no. 5 second order matrix elements is used. Data from JADE [9] and TPC [10] are shown in line 6 and 7. In the TPC data column no. 2 is for $0.3 < p_{Tout} < 0.5$ GeV and in column no. 3 also Λ's are included. Parton level results are shown in the three last lines, using a global z and $\alpha_s(p_T^2)$, in no. 8 for a conventional shower without three-jet matrix element; in no. 9 with matrix element correction included and in the final line also with coherence.

no.	all	all $p_{Tout} > 0.3$ GeV	$K^{\pm}$, p and $\bar{p}$	energy
1	1.22 ± 0.02	1.39 ± 0.05	1.50 ± 0.08	1.47 ± 0.02
2	1.19 ± 0.02	1.33 ± 0.05	1.56 ± 0.09	1.42 ± 0.02
3	1.22 ± 0.02	1.51 ± 0.06	1.59 ± 0.09	1.49 ± 0.03
4	1.22 ± 0.02	1.39 ± 0.05	1.43 ± 0.08	1.46 ± 0.03

5	1.30 ± 0.02	1.65 ± 0.05	1.71 ± 0.08	1.67 ± 0.02
6	1.39 ± 0.04	1.73 ± 0.13	1.90 ± 0.20	1.56 ± 0.04
7	1.19 ± 0.05	1.67 ± 0.24	1.58 ± 0.28	–
8	1.08 ± 0.03	1.27 ± 0.04	–	1.20 ± 0.03
9	1.04 ± 0.03	1.18 ± 0.05	–	1.18 ± 0.03
10	1.16 ± 0.03	1.17 ± 0.05	–	1.30 ± 0.03

Table 3

Average jet masses, calculated for a number of initial parton configurations, both on the parton and the hadron level. For ggg and ggγ events the angles between the jets are restricted to lie between 90^0 and 150^0.

no.	configuration	energy (GeV)	parton jet mass (GeV)	hadron jet mass (GeV)
1	$q\bar{q}$	29	5.3	6.5
2	gg	29	7.3	8.9
3	ggγ	50	7.5	9.5
4	ggg	50	6.8	8.7

Figure Captions

Fig. 1. Schematic diagram of parton shower evolution. The numbering of the first branches in an e^+e^- event is shown.

Fig. 2. Sphericity distribution for small values of S, illustrating the sensitivity to a too large m_{min}. Mark II data (points) [19], model results with m_{min} = 1 GeV (full line) and m_{min} = 4 GeV (dashed line). For both cases Λ = 0.4 GeV was used.

Fig. 3. Sphericity distribution illustrating the sensitivity to Λ. Mark II data (points) [19], model results with Λ = 0.2 GeV (dashed line), Λ = 0.4 GeV (full) and Λ = 0.6 GeV (dotted). A m_{min} = 1.5 GeV is used throughout.

Fig. 4. Sphericity distribution with a fixed α_s = 0.32 (dashed) and with $\alpha_s(m^2/4)$, Λ = 0.45 (dotted). As before, Mark II data (points) [19] and model results with $\alpha_s(p_T^2)$ (full line).

Fig. 5. The average gluon multiplicity as a function of energy. The local z, $\alpha_s(m^2/4)$ and conventional case (dash-dotted), with global z (dotted), with global z, $\alpha_s(p_T^2)$ and conventional evolution (long-dashed), and finally, the global z, $\alpha_s(p_T^2)$ and coherent evolution (full line). Analytical predictions for the coherent case [22], normalized to the comparable MC results at 10 GeV, are also shown (short-dashed).

Fig. 6. Analytical predictions for the mean gluon multiplicity, with conventional evolution and a light-cone z. Here β is a number, explained in the text, introduced to take care of the constraint $m_b + m_c \leqslant m_a$. Results are normalized to 5.0 at 10 GeV. Full line, results with β = 11·ln(2)/12 and dashed with β = 0.

Fig. 7. Ratio of mean charged multiplicity to parton multiplicity. Notation as in Fig. 5.

Fig. 8. The distribution in energy fraction $x = 2E/s^{1/2}$, plotted as $(x/\sigma)(d\sigma/dx)$. Notation as in Fig. 5.

Fig. 9. The same distribution as above for model results at 1 TeV with default values for Λ and m_{min} (full line), with m_{min} = 0.84 GeV (dashed), and for the MW model [8] (dotted).

Fig. 10. Rapidity distribution, $(1/\sigma)\cdot d\sigma(|Y|)/dY$, with the linear sphericity axis used as reference axis. Notation as in Fig. 5.

Fig. 11. Rapidity distribution as in Fig. 10, but for hadronized events. Coherent evolution (full line), conventional (dashed).

Fig. 12. The energy-energy correlation function at 6 TeV (forward-backward). Analytical predictions [28] (full line), local z and conventional evolution (dash-dotted), global z, conventional (dotted) and global z, coherent evolution (dashed). For model results, $\alpha_s(p_T^2)$ was consistently used.

Fig. 13. Ratios of consequtive opening angles at 100 GeV, plotted for local z and without coherence included (dash-dotted), with coherence (dotted), with global z and conventional evolution (dashed) and finally, global z and coherent case (full line). Here $\alpha_s(p_T^2)$ is consistently used.

Fig. 14. Distribution of the ratio of consecutive opening angles between jets, obtained with a cluster algorithm and history reconstruction described in the text. Results are binned in reconstructed jet mass. The points with full error bars is the coherent case and the dashed the conventional one. The error bars are statistical, and calculated from a sample of 12000 and 20000 events respectively.
a. At a CM energy of 200 GeV.
b. At a CM energy of 94 GeV.

Fig. 15. Aplanarity distribution at 50 GeV for continuum events (full line), gluonium events without parton showers (dashed line) and with parton showers included (dotted line).

Fig. 16. Particle flow at 50 GeV for continuum (full line) and onia (dashed), requiring a three-jet geometry. The most energetic jet is taken as reference angle (0^0) with the least energetic jet centered at largest angle.

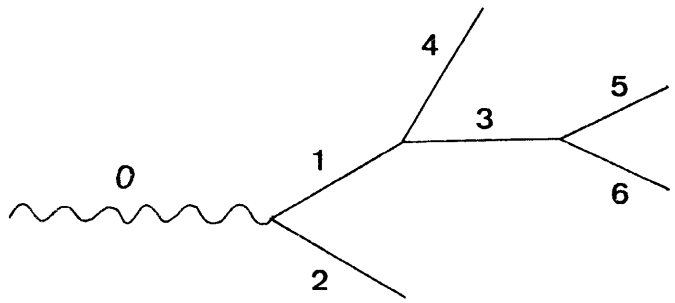

Fig 1

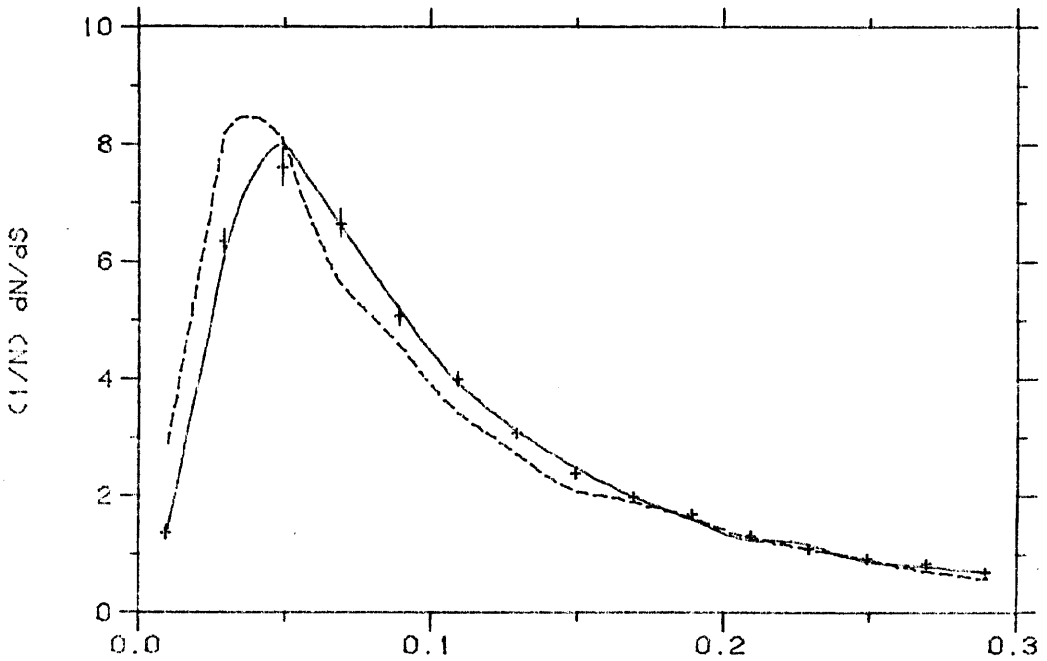

Sphericity
Fig 2

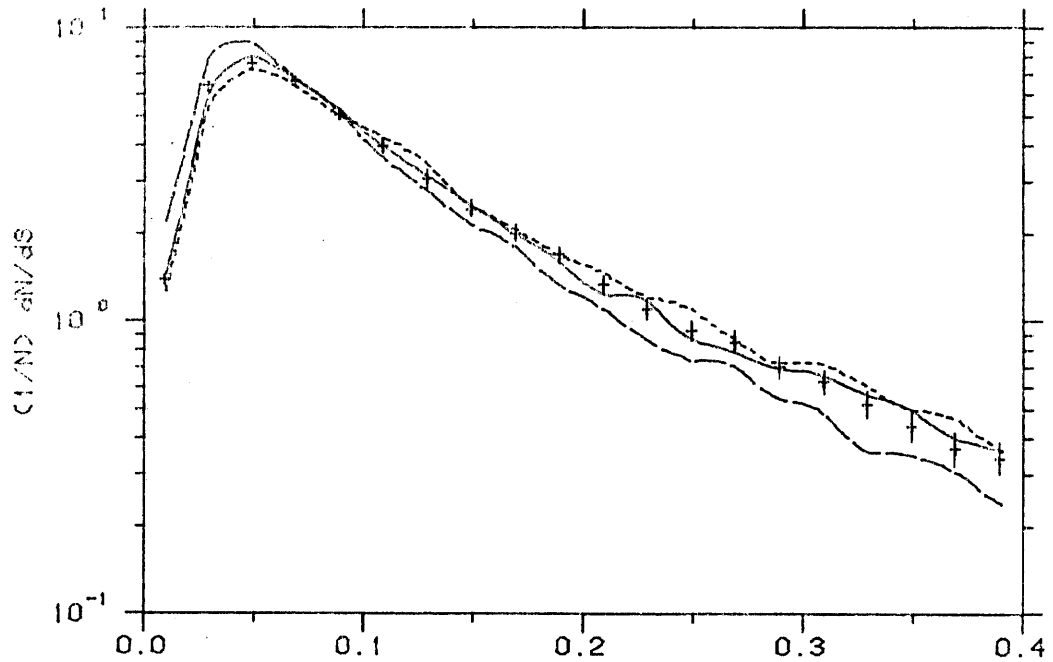

Sphericity
Fig 3

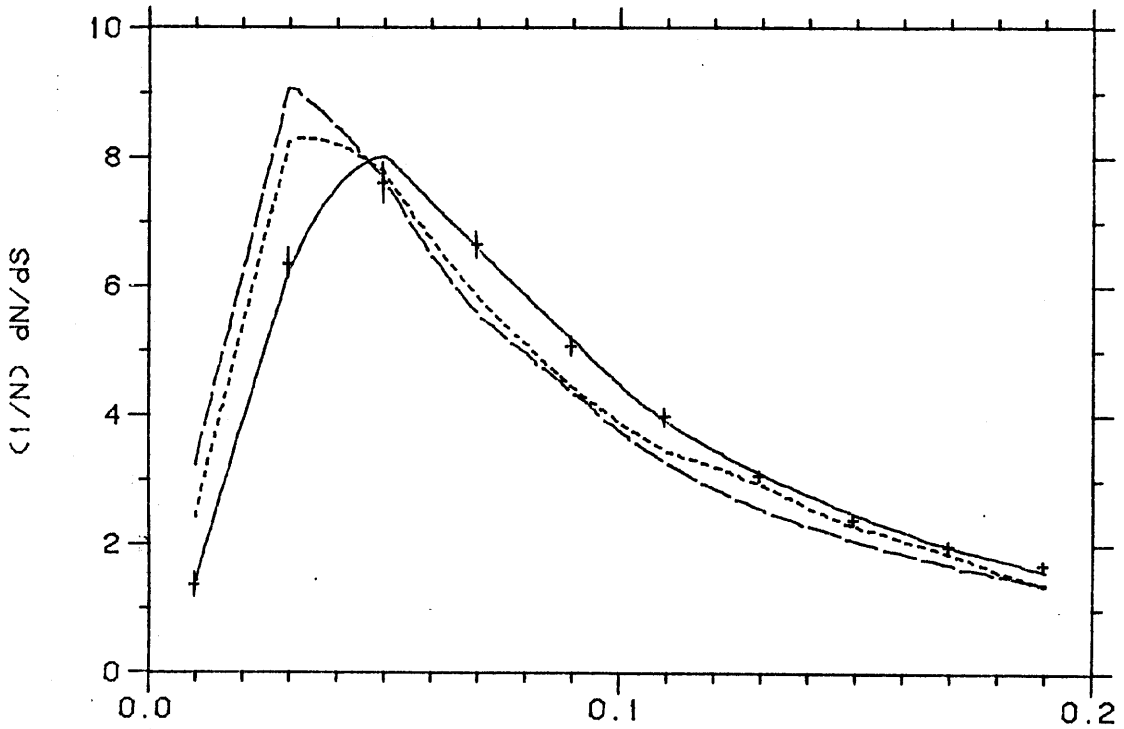
10
8
6
4
2
0
0.0
0.1
0.2
(1/N) dN/dS
Sphericity

Fig 4

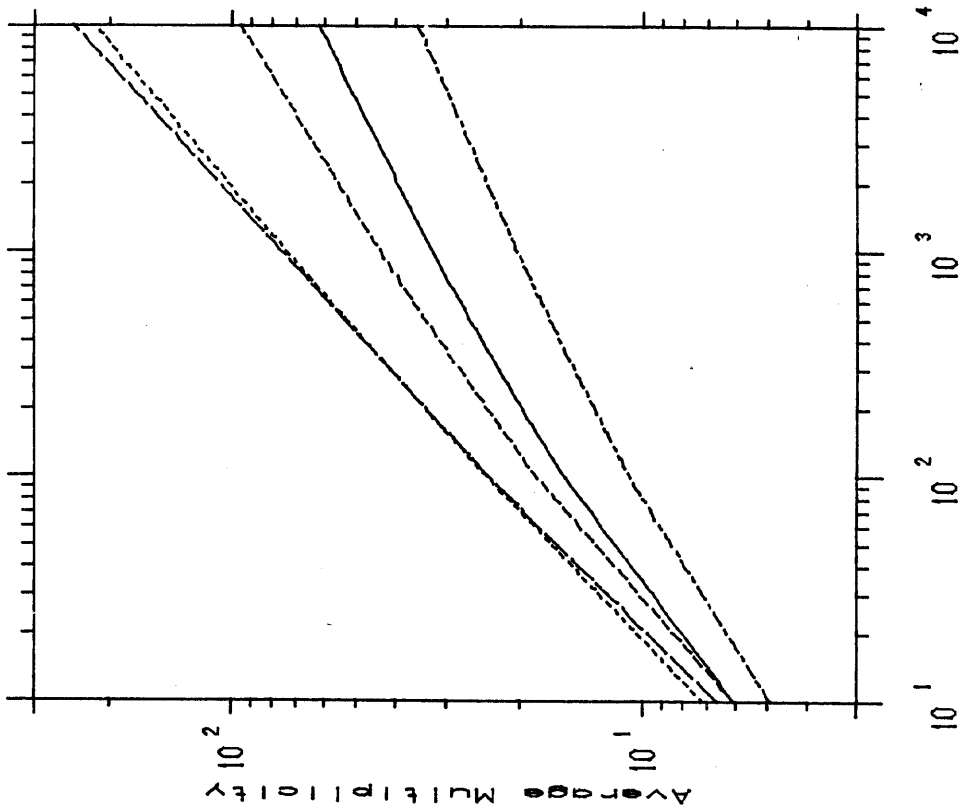
Average Multiplicity
10^2
10^1
10^1
10^2
10^3
10^4
Energy (GeV)

Fig 5

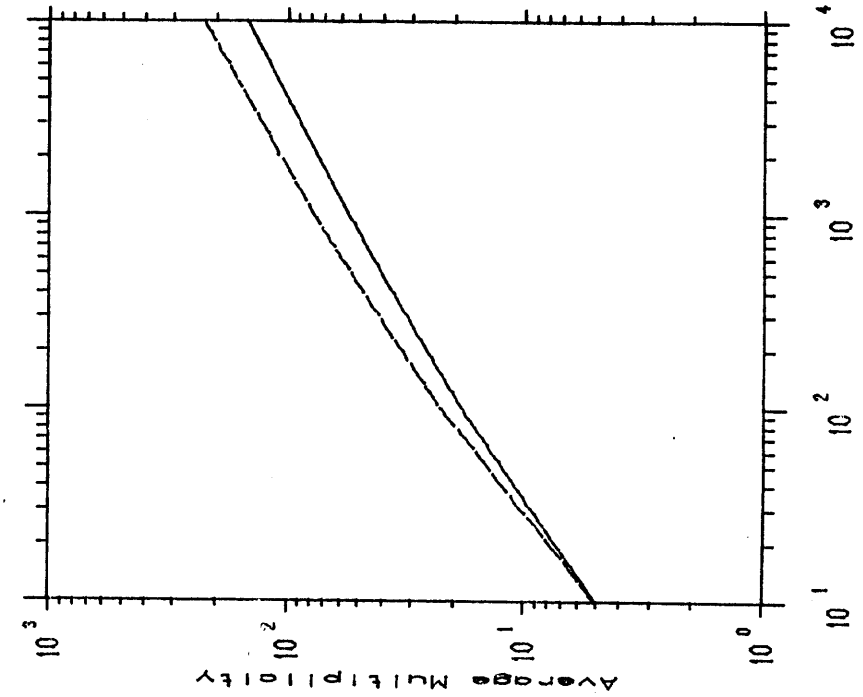
Average Multiplicity
10^{3}
10^{2}
10^{1}
10^{0}
10^{1}
10^{2}
10^{3}
10^{4}
Energy (GeV)

Fig 6

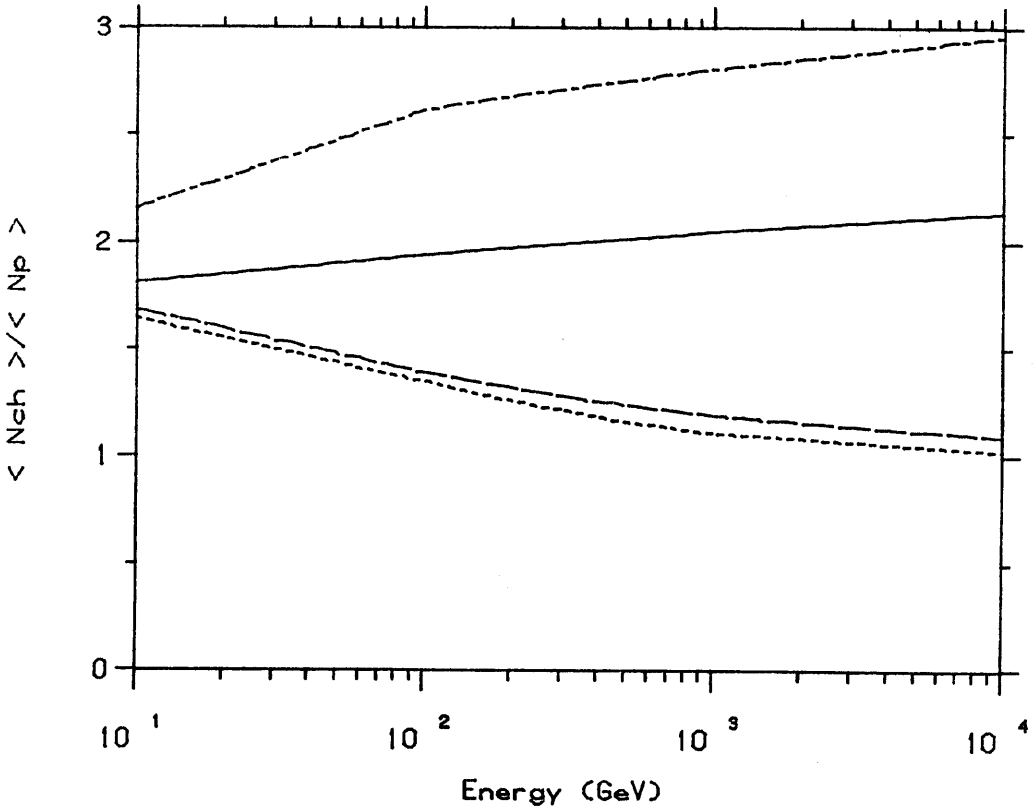
< Nch >/< Np >
0
1
2
3
10^{1}
10^{2}
10^{3}
10^{4}
Energy (GeV)

Fig 7

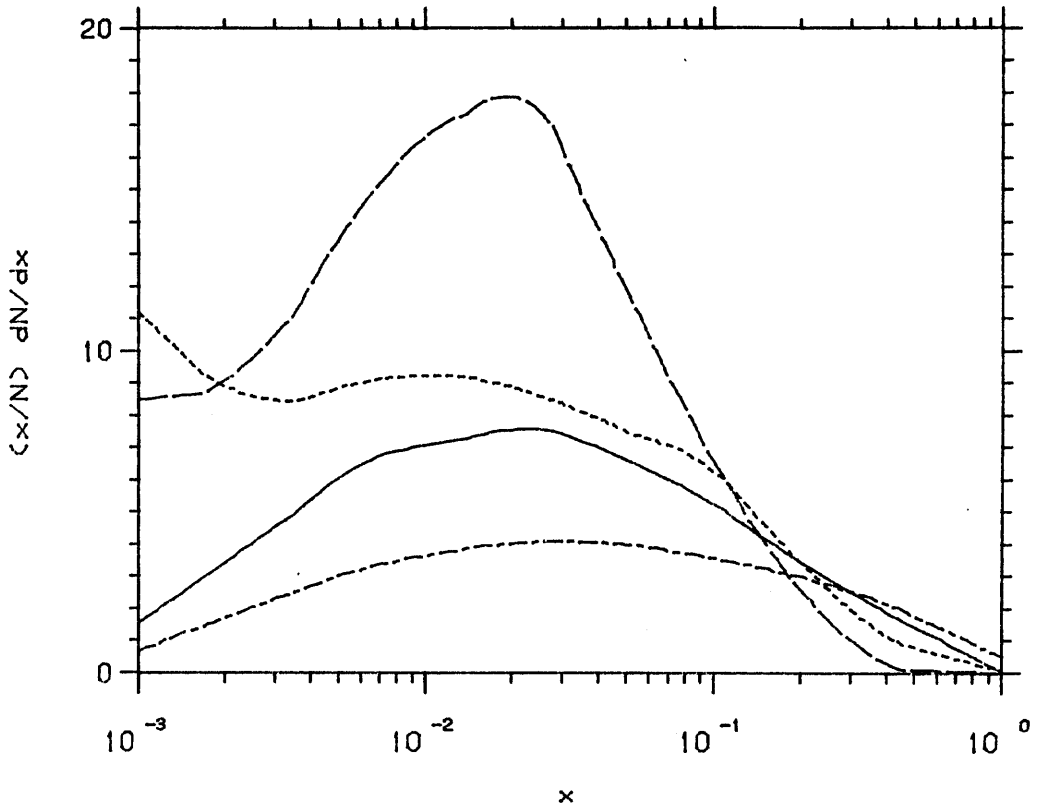

Fig 8

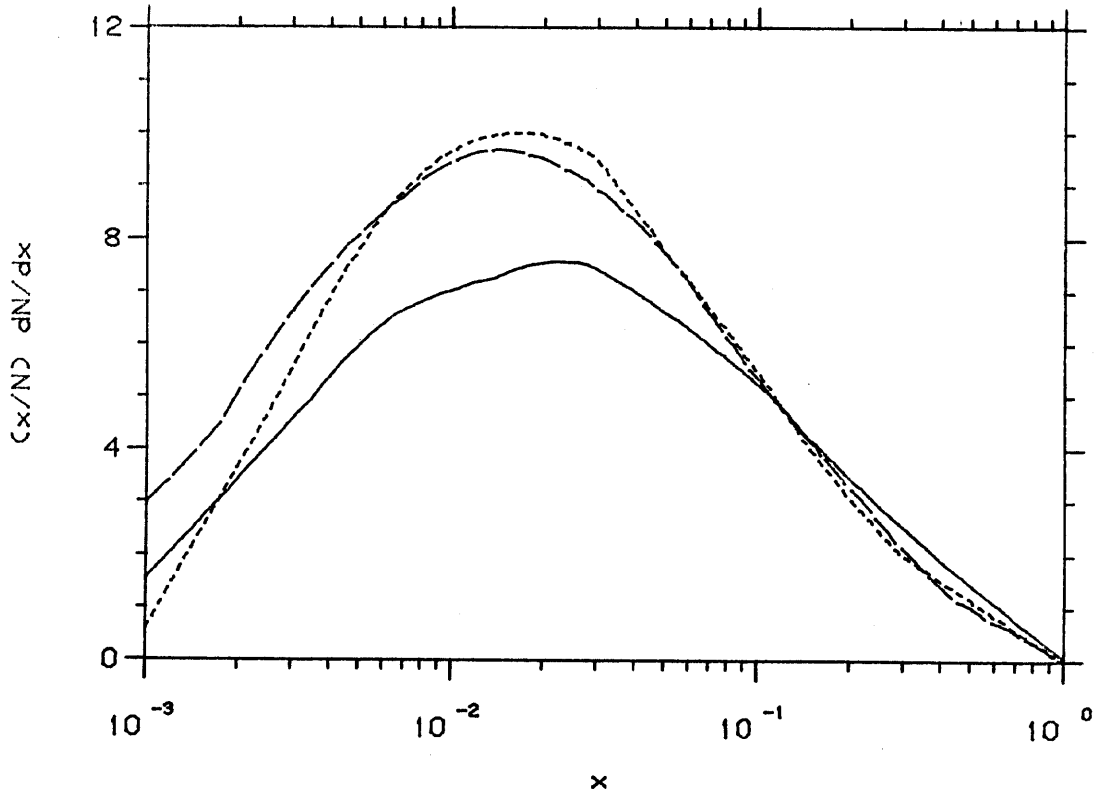

Fig 9

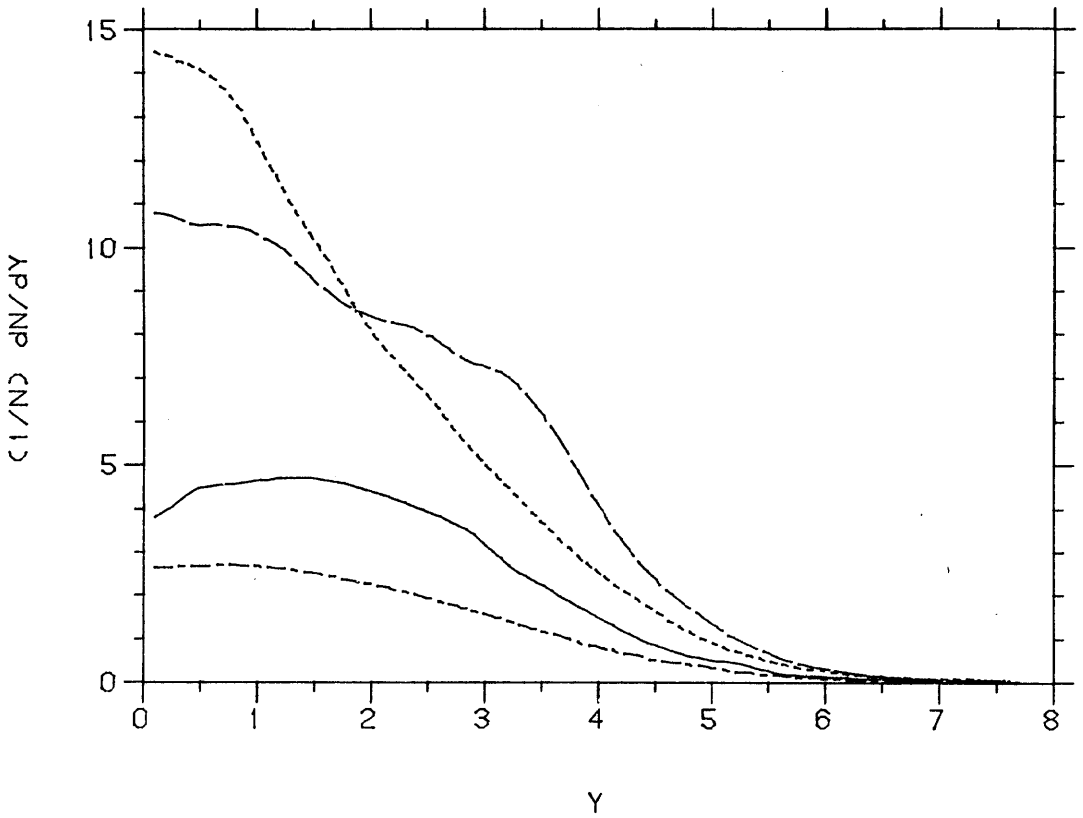

Fig 10

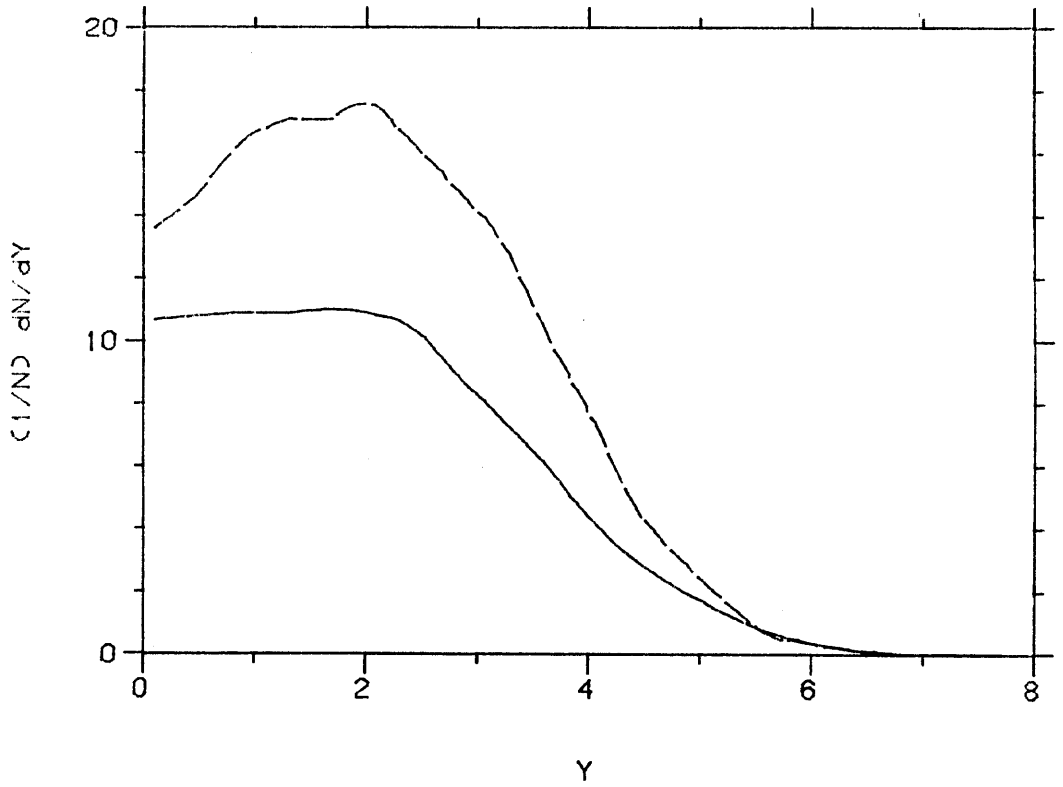

Fig 11

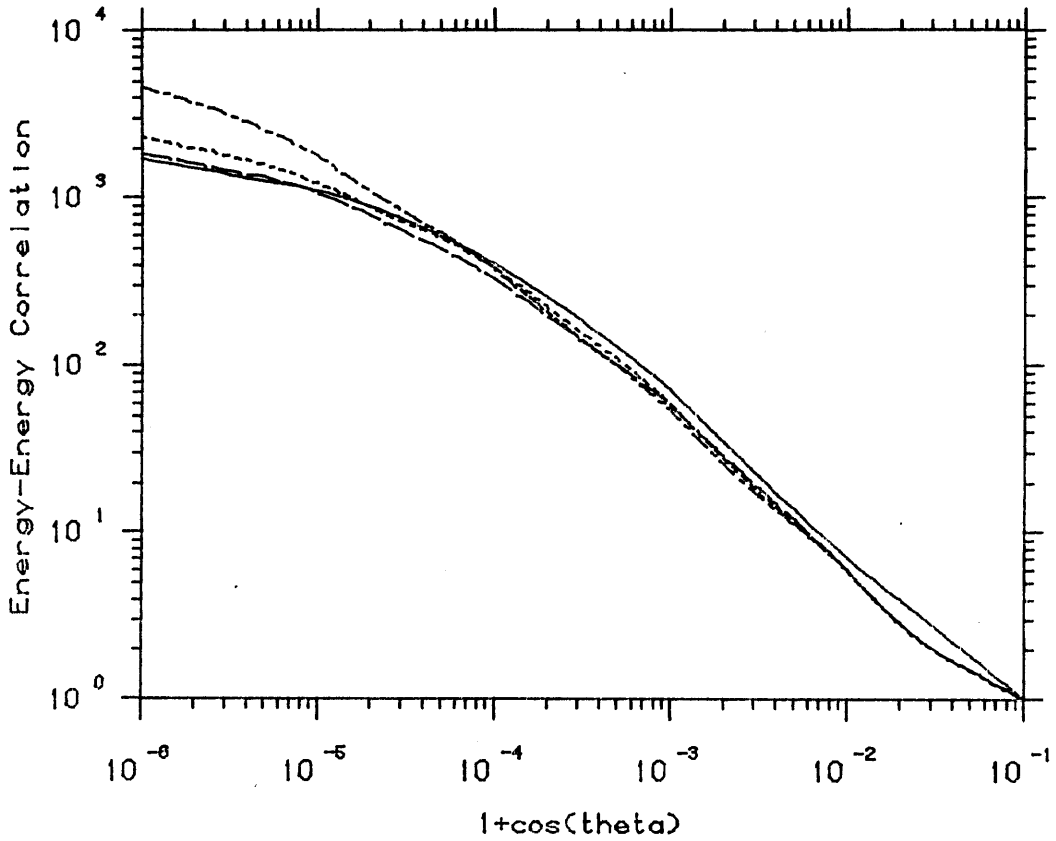

Fig 12

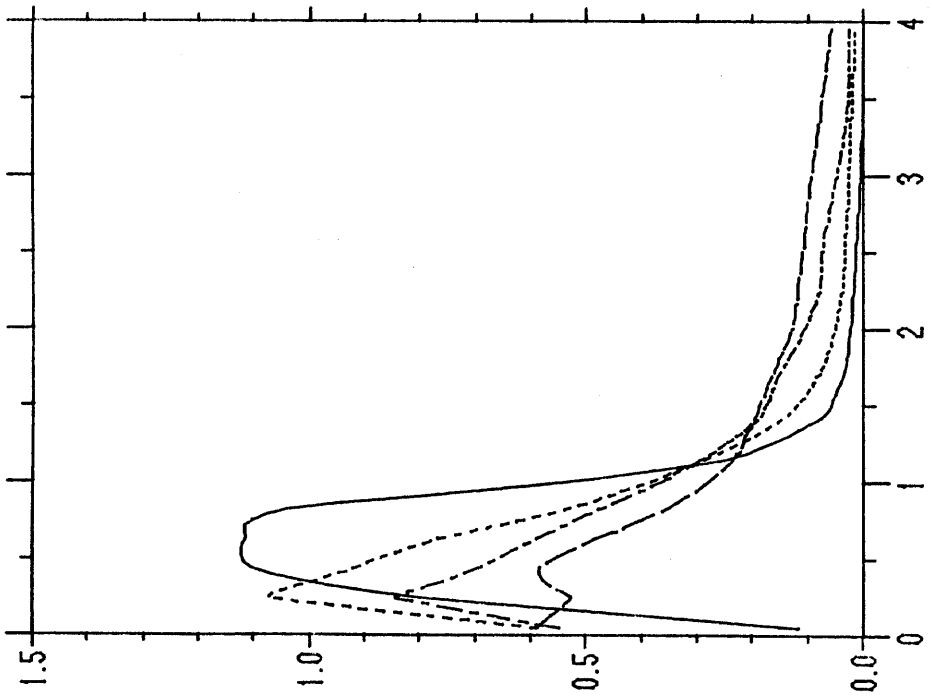

Ratio of Angles

Fig 13

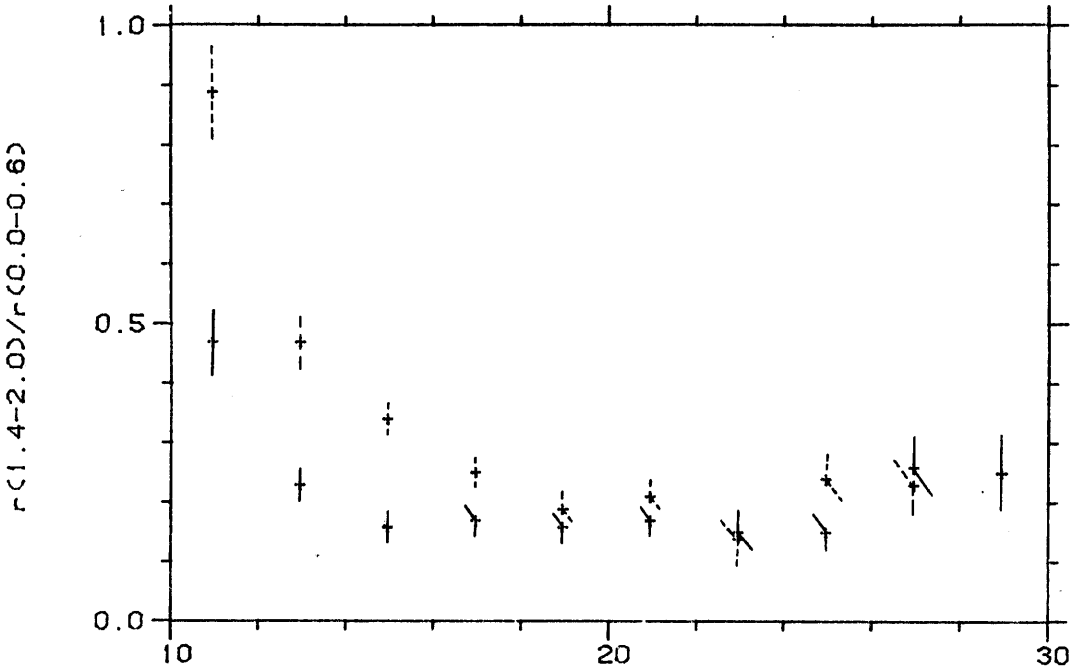

Jet mass
Fig 14 a

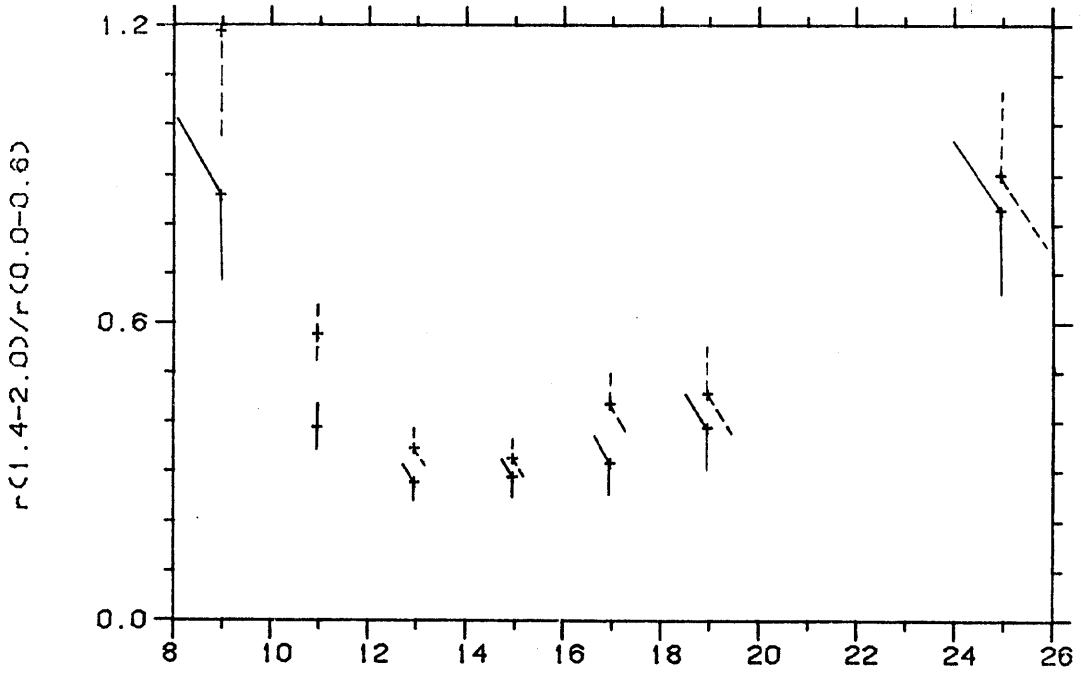

Jet mass
Fig 14 b

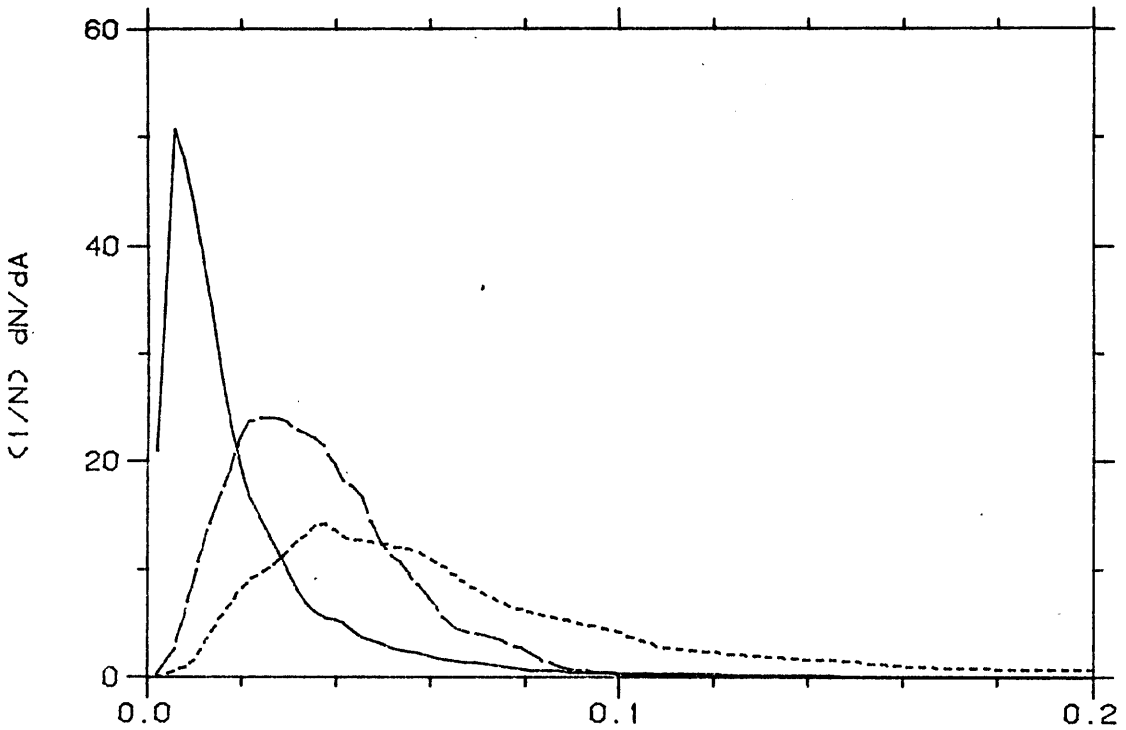

Aplanarity
Fig 15

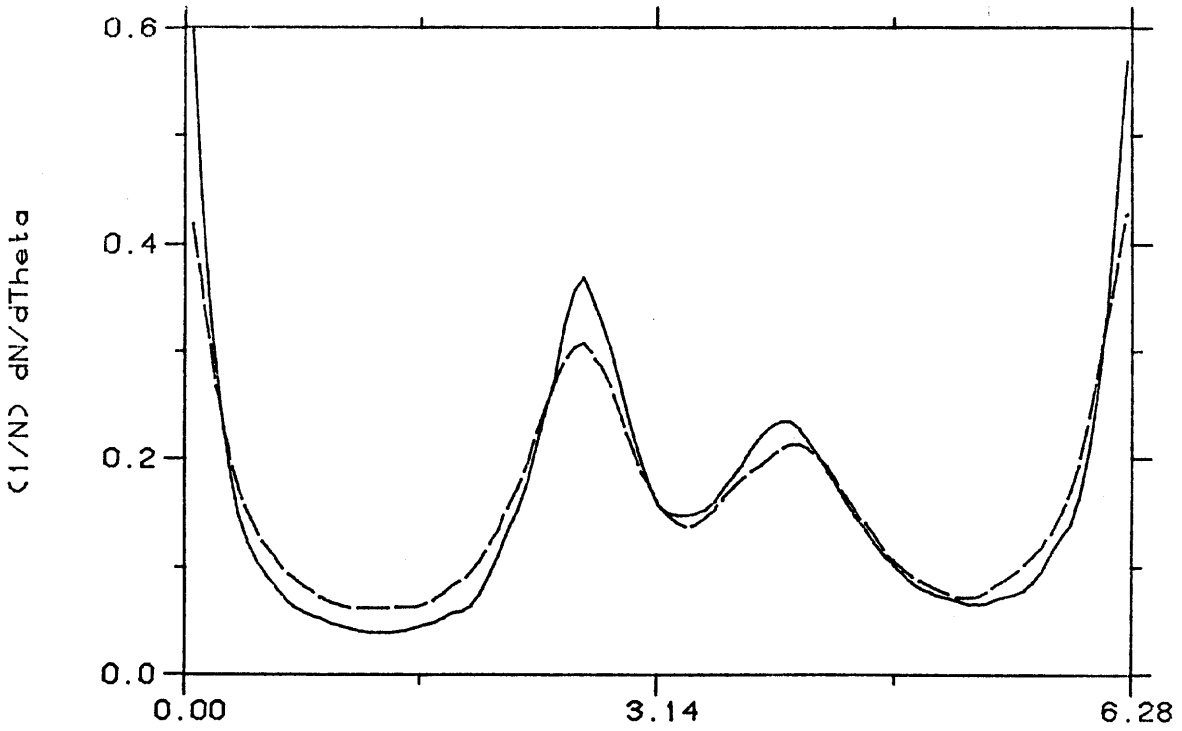

Theta
Fig 16